

Z (1996)



## This is to certify that the

## thesis entitled

A QUALITATIVE EXAMINATION OF STRAIN USING ELECTRON BACKSCATTERING PATTERNS EMPLOYING A 35MM CAMERA BODY IN A SCANNING ELECTRON MICROSCOPE

presented by

ALAN W. GIBSON

has been accepted towards fulfillment of the requirements for

M.S. degree in MATERIALS SCIENCE

Major professor

Date Sept 5, 1995

**O**-7639

MSU is an Affirmative Action/Equal Opportunity Institution

## LIBRARY Michigan State University

PLACE IN RETURN BOX to remove this checkout from your record.
TO AVOID FINES return on or before date due.

DATE DUE	DATE DUE	DATE DUE
·		

MSU is An Affirmative Action/Equal Opportunity Institution cyclestatedus.pm3-p.1

# A QUALITATIVE EXAMINATION OF STRAIN USING ELECTRON BACKSCATTERING PATTERNS EMPLOYING A 35MM CAMERA BODY IN A SCANNING ELECTRON MICROSCOPE

By

Alan W. Gibson

## A THESIS

Submitted to
Michigan State University
in partial fulfillment of the requirements
for the degree of

MASTER OF SCIENCE

Department of Materials Science and Mechanics

1995

#### **ABSTRACT**

## A QUALITATIVE EXAMINATION OF STRAIN USING ELECTRON BACKSCATTERING PATTERNS EMPLOYING A 35MM CAMERA BODY IN A SCANNING ELECTRON MICROSCOPE

By

#### Alan W. Gibson

A comparison was made between two electron backscattering pattern (EBSP) recording systems. A system utilizing a 35mm camera body in an Hitachi S2500 scanning electron microscope (SEM), incorporating film transfer and exposure control, proved far superior in providing high quality EBSP images to a commercial LINK system incorporating a phosphor screen, low light television camera, and SEMPER image processing software. Also, EBSPs have been used to determine the appropriate amount of electropolishing required to obtain strain free material in commercially pure aluminum. EBSP quality, known to deteriorate with increasing strain, was shown to visually improve with increasing electropolishing time. Next, EBSPs have been used to qualitatively examine strain in commercially pure aluminum as a function of distance away from a surface that has been damaged by mechanical grinding. Visual comparisons showed an improvement in pattern quality away from the damaged surface. Additionally, EBSPs have been used to qualitatively investigate strain in a (Al<sub>2</sub>O<sub>3</sub>)<sub>p</sub>/6061 aluminum alloy metal matrix composite as a function of distance away from an  $(Al_2O_3)$  particulate. The EBSP technique was found to be inappropriate due to the material's small grain size.

To Barbara...

my loving wife, best friend,

and eternal companion

## **ACKNOWLEDGEMENTS**

This study was made possible by funding from the National Science Foundation, grant DMR-9257826.

I would like to thank Dr. Martin A. Crimp for his guidance, friendship, and many interesting, informative discussions on countless subjects. His hard work and dedication have been an inspiration. I would like to thank Leo Szafranski, Machine Shop Technician, for aiding me with his expert craftsmanship. Thanks, also, are extended to the MSM office staff including Iris Taylor, Joann Peterson, Debbie Conway, and Lorna Coulter. In addition, I owe gratitude to Pat, Dean, Julian, Ojars and my other lab cohorts, as well as to all international students with whom I have had many interesting and informative discussions.

Foremost, however, I would like to thank God for His forgiveness.

## TABLE OF CONTENTS

List of Tables	vii
List of Figures	viii
Introduction	1
1. Literature Review	3
1.1 What are EBSPs & how are they formed	3
1.2 How and why are EBSPs used	21
1.3 EBSP recording systems	25
1.4 Sample Preparation	30
1.5 Objectives	39
2. Experimental Procedure	41
2.1 Material	41
2.2 Sample Preparation	41
2.2.1 GaAs	41
2.2.2 Commercially pure Al and $(Al_2O_3)_p/6061$ aluminum	41
2.3 Camera Systems	45
2.3.1 35mm Camera/Sample Set-up	45
2.3.2 Link Merlin EBSP Camera System/Sample Set-up	48
2.4 Acquiring EBSPs	48
2.5 EBSP Experiments	50
2.5.1 Recording EBSPs using different films in the 35mm camera body	50

2.5.2 LINK Merlin EBSP Camera System vs. 35mm camera using GaAs and commercially pure Al specimens	50
2.5.3 EBSPs recorded after 5 minutes and after 25 minutes of electropolishing using a commercially pure Al specimen	51
2.5.4 EBSPs recorded as a function of distance away from a surface that has been damaged by mechanical grinding with a 180 grit sandbelt using a commercially pure Al specimen	51
2.5.5 EBSPs recorded as a function of distance away from an (Al <sub>2</sub> O <sub>3</sub> ) particulate in a (Al <sub>2</sub> O <sub>3</sub> ) <sub>p</sub> /6061 aluminum alloy specimen	53
3. Experimental Results and Discussion	55
3.1 EBSPs recorded on 4 different films	56
3.2 LINK Merlin EBSP camera system vs. 35mm camera using GaAs and commercially pure Al specimens	60
3.3 EBSPs recorded after 5 minutes and after 25 minutes of electropolishing using a commercially pure Al specimen	66
3.4 EBSPs recorded as a function of distance away from a surface that has been damaged by mechanical grinding with a 180 grit sandbelt using a commercially pure Al specimen	68
3.5 EBSPs recorded as a function of distance away from an (Al <sub>2</sub> O <sub>3</sub> ) particulate in an (Al <sub>2</sub> O <sub>3</sub> ) <sub>p</sub> /6061 aluminum alloy specimen	77
4. Conclusions	83
List of References	85

## LIST OF TABLES

Table		Page
1	Backscatter coefficients, $\eta$ , in percentages, as a function of atomic number and electron energy, E, for normal incidence.	8

## LIST OF FIGURES

Figure		Page
1	Backscatter coefficient, $\eta$ , as a function of atomic number, at 20 keV electron energy.	5
2	Backscatter coefficient, $\eta$ , as a function of atomic number, plotted for a range of electron beam energies.	7
3	Backscatter coefficient, $\eta$ , as a function of tilt, $\theta$ , for several elements as calculated by Monte Carlo simulation at 20 keV electron beam energy.	9
4	Schematic illustrating the increase in backscattered electrons due to tilting the specimen with respect to the incident electron beam.	11
5	Diagram illustrating backscattered electron trajectories produced when an electron beam is incident normal to a specimen and to a specimen tilted at 70°.	12
6	Schematic illustrating the inelastic collisions, Bragg diffraction, and resultant formation and imaging of Kikuchi lines as a result of an incident electron beam.	15
7	Schematic illustrating the inelastic collisions, Bragg diffraction, and resultant formation and imaging of EBSPs as a result of an incident electron beam.	16
8	The formation of EBSP bands, on a macroscopic level, resulting from an electron beam incident upon a tilted specimen, and their intersection with an imaging medium.	18
9	The formation and imaging of EBSPs as a result of backscattered electrons diffracting from a (1 -1 0) plane and the correspondence of the [0 0 1] and [1 1 2] directions with locations on the EBSP.	20
10	Cylindrical chamber used, in one of the first published instances, to record electron backscattering patterns.	26

11	Current as a function of voltage representative of the relationship seen when electropolishing aluminum in perchloric acid based electrolytes.	34
12	Current as a function of voltage representative of the more complex relationship seen when the potential exists for etching, polishing, and pitting.	35
13	Diagram of electropolishing cell.	44
14	Specimen/camera configuration, shown in the retracted position, mounted on the SEM goniometer stage.	46
15	Commercially pure Al sample showing the mechanically ground surface and the electropolishing surface of interest upon which EBSPs were performed as a function of distance away from the damaged surface.	52
16	(Al <sub>2</sub> O <sub>3</sub> ) <sub>p</sub> /6061 aluminum matrix sample showing the (Al <sub>2</sub> O <sub>3</sub> ) particulate away from which EBSPs were performed as a function of distance.	54
17	EBSP images of GaAs recorded with the 35mm camera body system, using Kodak's (a) TMax <sup>TM</sup> 3200, (b) TMax <sup>TM</sup> 400, (c) Technical Pan <sup>TM</sup> , and (d) Fine Grain Release Positive <sup>TM</sup> film.	57-58
18	EBSP images of GaAs recorded using the (a) commercial LINK Merlin EBSP camera system with no image processing, (b) commercial LINK Merlin EBSP camera system coupled with Semper 6.4 image processing of 15 seconds of frame averaging, and (c) 35mm camera body system.	61-62
19	EBSP images of commercially pure Al recorded using the (a) commercial LINK Merlin EBSP camera system with no image processing, (b) commercial LINK Merlin EBSP camera system coupled with Semper 6.4 image processing of 15 seconds of frame averaging, and (c) 35mm camera body system.	64-65
20	EBSP images of commercially pure Al recorded using the 35mm camera body system and Fine Grain Release Positive <sup>TM</sup> film after (a) 5 minutes of electropolishing (b) 25 minutes of electropolishing	67

- 21 EBSP images of commercially pure Al recorded, using the 35mm camera body system and Fine Grain Release Positive<sup>TM</sup> film, at (a) the damaged edge, (b) 1.0 micron, (c) 2.0 microns, (d) 4.0 microns, (e) 5.0 microns, (f) 8.0 microns, (g) 10.0 microns, (h) 12.0 microns, (i) 15.0 microns, (j) 20.0 microns, (k) 25.0 microns, and (l) 30.0 microns from the damaged edge.
- 22 EBSP images of (Al<sub>2</sub>O<sub>3</sub>)<sub>p</sub>/6061 aluminum alloy recorded, using the 35mm camera body system and Fine Grain Release Positive<sup>TM</sup> film, at (a) the (Al<sub>2</sub>O<sub>3</sub>)<sub>p</sub>/6061 matrix interface, and at (b) 1.0 micron, (c) 2.0 microns, (d) 5.0 microns, and (e) 8.0 microns away from the (Al<sub>2</sub>O<sub>3</sub>)<sub>p</sub>/6061 matrix interface.

78-80

70-75

#### INTRODUCTION

Diffraction studies often are carried out using transmission electron microscopy, X-ray diffraction, electron channelling pattern, and electron backscattering pattern (EBSP) techniques. Of these techniques, EBSPs are becoming increasingly popular due to their advantages.

EBSPs have exceptional spatial and angular resolution. Furthermore, the relatively easy sample preparation necessary to obtain patterns combined with the ease of experimentally obtaining patterns and crystallographic information has led to the increasing use of the EBSP technique in materials studies. Furthermore, unlike TEM related techniques, EBSPs may be obtained from bulk specimens. The EBSP method is capable of submicron resolution and is used for local crystallographic measurements, phase identification, local texture measurements, and strain quantification/qualification.

The formation of EBSPs is directly dependent upon the material's crystallography, and therefore, various interpretations of the EBSPs can reveal extensive information related to the crystallography of the sample. The distribution, orientation, and delineation of the EBSP reveals information about the distribution, orientation, and crystallinity of the atomic planes in the sample.

The delineation of the EBSP bands is dependent upon crystal perfection and therefore can yield localized information on dislocation density, stacking fault densities, or point defect concentrations. The lattice defects are responsible for causing a local bending of the lattice planes, thereby causing a diffuseness in the

EBSP band edges. An increasing number of lattice defects causes an increasing diffuseness in the band edges.

The current study takes advantage of the increased band edge diffuseness by using EBSPs to study different deformation scenarios. EBSPs are used to qualitatively examine deformation in commercially pure aluminum as a function of distance away from a surface that has been damaged by mechanical grinding. In another experiment, EBSPs are used to study deformation as a function of distance away from an Al<sub>2</sub>O<sub>3</sub> particulate in an (Al<sub>2</sub>O<sub>3</sub>)<sub>p</sub>/6061 aluminum alloy matrix.

Additionally, EBSPs are used to study the effects of electropolishing on EBSP pattern quality using a commercially pure aluminum specimen.

Other preliminary studies are made to find a superior, electron sensitive 35mm film to use in the current examinations. Furthermore, a comparison is made between two EBSP recording systems. One system incorporates a commercial LINK Merlin EBSP lowlight TV camera coupled to a phosphor screen. The other recording system uses a 35mm camera, mounted within the SEM vacuum chamber, and records EBSPs directly on film.

#### 1. LITERATURE REVIEW

## 1.1 What are EBSPs & how are they formed

## Signals in the SEM

In a scanning electron microscope (SEM), electrons are accelerated down the column through a series of electromagnetic lenses and strike a sample [1, 2]. After the primary incident electron beam strikes the sample in the SEM, the interactions of these electrons with the sample produce different types of signals. These signals may be used to form images and/or perform some type of analysis on the sample. The signals are produced by electron interaction events which may be categorized as being either elastic or inelastic.

As described in more detail by Goldstein et al. [3], in an inelastic collision, there is some transfer of energy from an incident electron to an electron in the sample. This transfer of energy may be extremely small, or may include a total transfer of the incident electron's energy. Secondary electrons, Brehmsstrahlung X-rays, and inner shell ionization are examples of the signals produced by inelastic events.

### **Backscattered Electrons**

In an elastic collision, there is no transfer of energy from an incident electron to an electron in the sample. These types of collisions give rise to backscattered electrons. Backscattered electrons are strictly defined as being single, elastically scattered electrons whose trajectory is changed by more than 90° from the forward trajectory of the incident electrons and whose exit surface is the same as it's entry surface [3].

The fraction of incident electrons that are backscattered can be described by the backscatter coefficient,  $\eta$ , which is defined in Equation 1 as:

$$\eta = \frac{\eta_{BSE}}{\eta_B} = \frac{i_{BSE}}{i_B} \tag{1}$$

where  $\eta_B$  is the number of electrons incident on the sample surface,  $\eta_{BSE}$  is the number of backscattered electrons,  $i_B$  is the current of electrons impinging onto the sample, and  $i_{BSE}$  is the current of electrons being backscattered out of the sample. Though beyond the scope of this research, a solid state physics theoretical approach to the understanding of backscattered electrons as been attempted by Dudarev *et al.* [4].

Goldstein et al. [3] and Reimer [5] explain in great detail the dependence of  $\eta_{BSE}$ , the number of backscattered electrons produced, on many experimental and material parameters. The atomic number, Z, of the sample under investigation strongly effects  $\eta_{BSE}$ , thus effecting  $\eta$ . A plot of backscattered coefficient versus atomic number reveals a strong monotonic increase in  $\eta$  with increasing Z, as shown in Figure 1. Figure 1 assumes an electron energy of 20 keV. The curve of  $\eta$  vs. Z can be fit with Equation 2 as

$$\eta = -0.0254 + 0.016Z - [1.86x10^{-4}]Z^2 + [8.3x10^{-7})]Z^3$$
 (2)

where  $\eta$  and Z are as noted above. It should be noted, however, that a closer

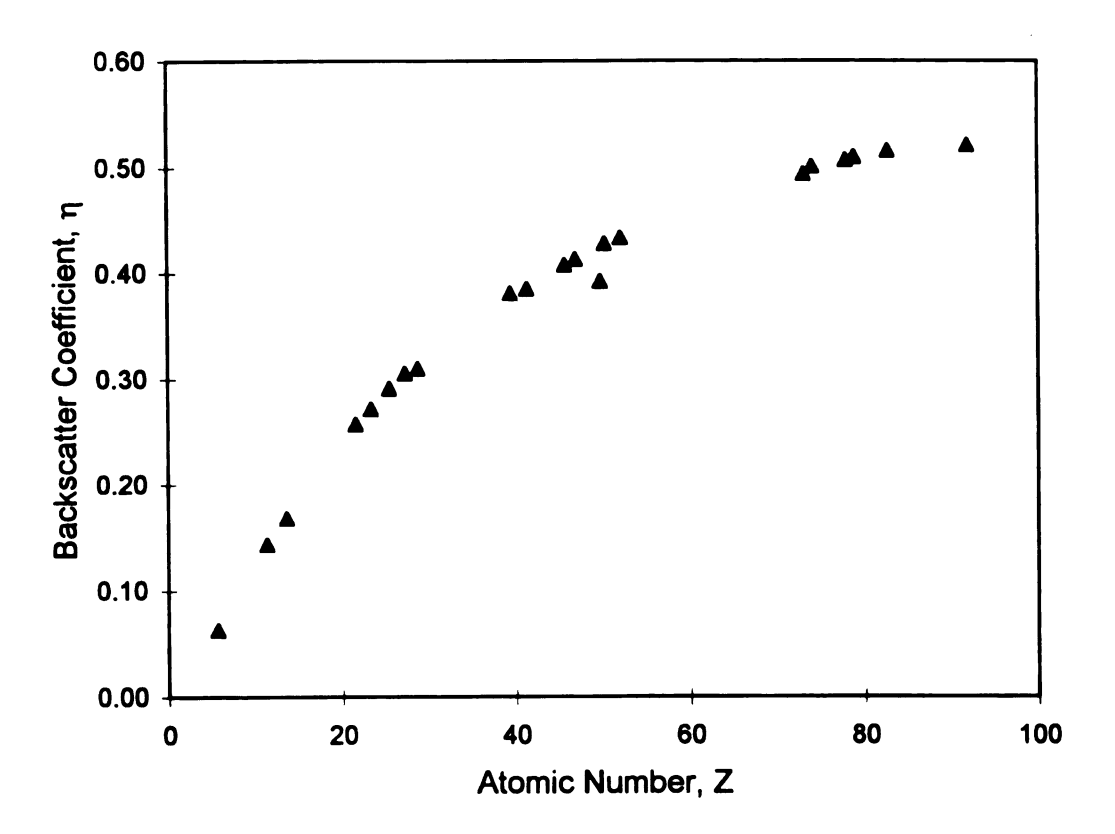


Figure 1

Backscatter coefficient,  $\eta$ , as a function of atomic number, at 20 keV electron energy. Adapted from [3].

examination of this curve would show that small increases in Z would not necessarily correspond to a higher  $\eta$ . When the material is a homogeneous mixture of elements on the atomic level,  $\eta$  follows a simple rule of mixtures described by Equation 3

$$\mathbf{\eta} = \sum_{i} C_{i} \mathbf{\eta}_{i} \tag{3}$$

where  $C_i$  is the mass concentration of the individual constituents and  $\eta_i$  is the pure elemental backscatter coefficient.

Figure 2 (plotted for a range of beam energies) demonstrates that the backscatter coefficient depends on incident electron beam energy to only a slight degree. This appears contrary to what would be expected purely from a Monte-Carlo trajectory prediction [3]. Interestingly, some elements such as Al actually show a decrease in  $\eta$  with increasing electron energy, as shown in Table 1.

An important feature, utilized to great advantage in this study, is the dependence of  $\eta$  upon sample tilt [3]. Figure 3 demonstrates the reliance of  $\eta$  on the specimen tilt for several elements. This dependence may be fitted with the expression in Equation 4

$$\eta(\theta) = 1/(1 + \cos\theta)^{P}$$
 (4)

where the tilt angle,  $\theta$ , on the X-axis is the complement of the smaller angle between

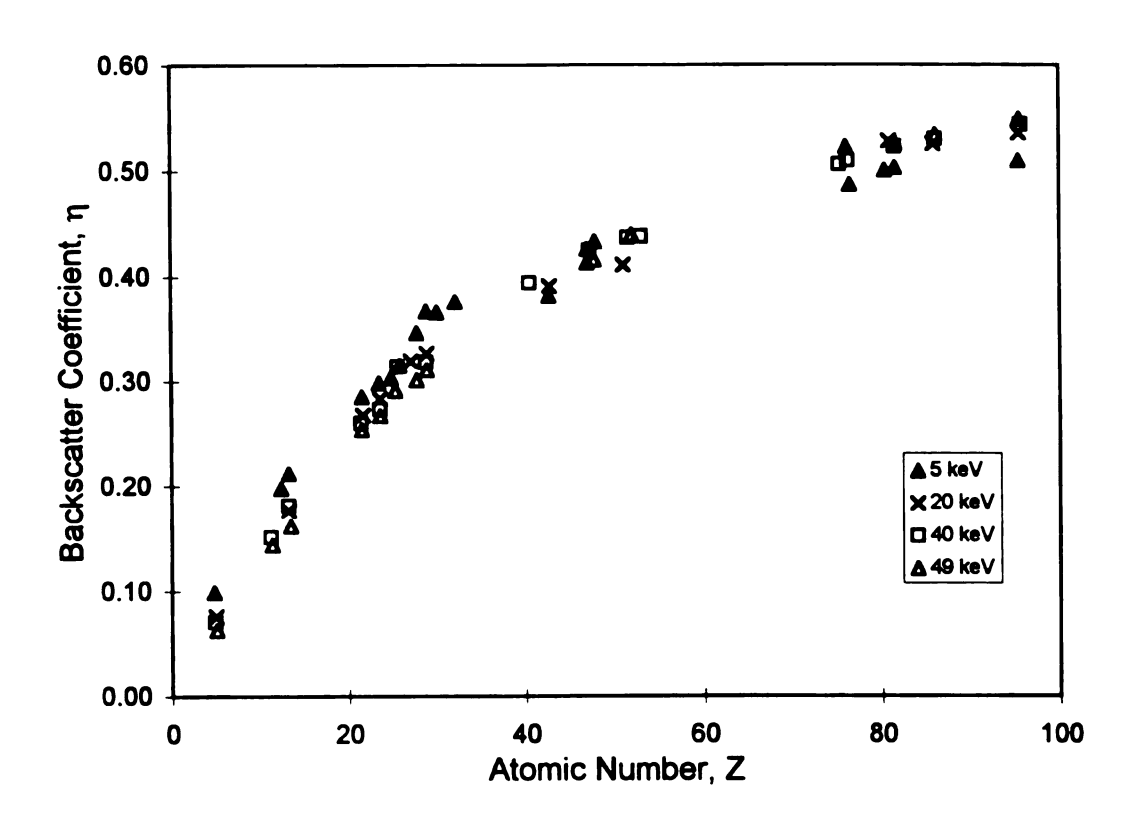


Figure 2 Backscatter coefficient,  $\eta$ , as a function of atomic number, plotted for a range of electron beam energies. Adapted from [3].

Table 1

Backscatter coefficients,  $\eta$ , in percentages, as a function of atomic number and

electron energy, E, for normal incidence. Adapted from [5].

ΑI E[keV] Cu Au Be 17.5 31.3 9.3 5 47.8 11.0 5 17.1 31.0 48.0 13.4 5 16.4 31.4 49.1 17.3 5 15.9 31.0 49.2 25.2 4.5 15.1 30.7 50.1 41.5 14.5 30.1 50.7 4 62.1 4 13.7 51.3 29.9 4 81.8 13.5 51.0 29.4 102.0 13.3 29.1 51.3 3.5

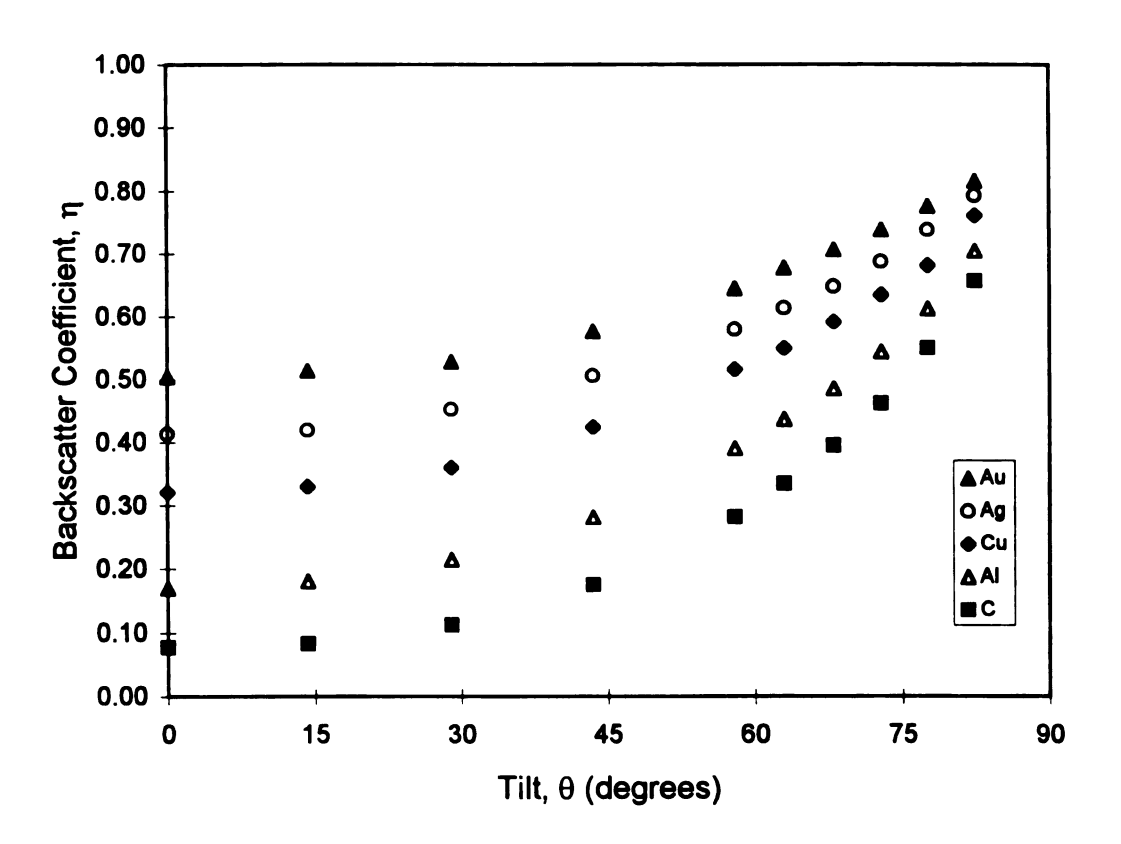


Figure 3

Backscatter coefficient,  $\eta$ , as a function of tilt,  $\theta$ , for several elements as calculated by Monte Carlo simulation at 20 keV electron beam energy. Adapted from [3].

the electron beam and the specimen plane, and  $P = 9/Z^{1/2}$ . A purely geometrical argument reveals that changing the angle of beam incidence by sample tilt is the same as shifting the trajectory of the backscatter electron cone. Figure 4 schematically illustrates this shifting of the electron cone trajectory when altering the sample tilt from 0° to near 70°, where an electron has an equal probability of landing anywhere on the darkened base of the cone. The effect of tilting the sample is now obvious in that more backscatter electrons are able to escape the surface due to simple geometric advantage. The conical shape, in this instance, is indicative of the general shape of the electron trajectories as given by Monte Carlo simulations. The Monte Carlo Simulation in Turbo Pascal program [6] demonstrates that at a beam energy of 25 keV, using aluminum's atomic number, weight, and density, the backscatter coefficient increases with increasing sample tilt. At 0° tilt, i.e. beam perpendicular to sample surface,  $\eta = 0.160$ ; at 30° tilt,  $\eta = 0.170$ ; at 60° tilt,  $\eta = 0.400$ ; and at 70° tilt,  $\eta = 0.470$ .

Tilting of the sample not only increases the number of backscattered electrons, but also increases their tendency for forward scattering and changes their angular distribution, as shown in Figure 5. Forward scattering occurs when the electron trajectories continue in approximately the same direction as the electron beam. Thus, as the sample is tilted, the backscatter electron signal is stronger in directions away from the incident beam and a detector placed in this appropriate position will register a much higher amount of backscattered electrons, resulting in a higher  $\eta$  than if it were placed elsewhere. A beam incident on a specimen tilted at 70° produces backscattered electrons that follow a more forward trajectory than if the specimen had

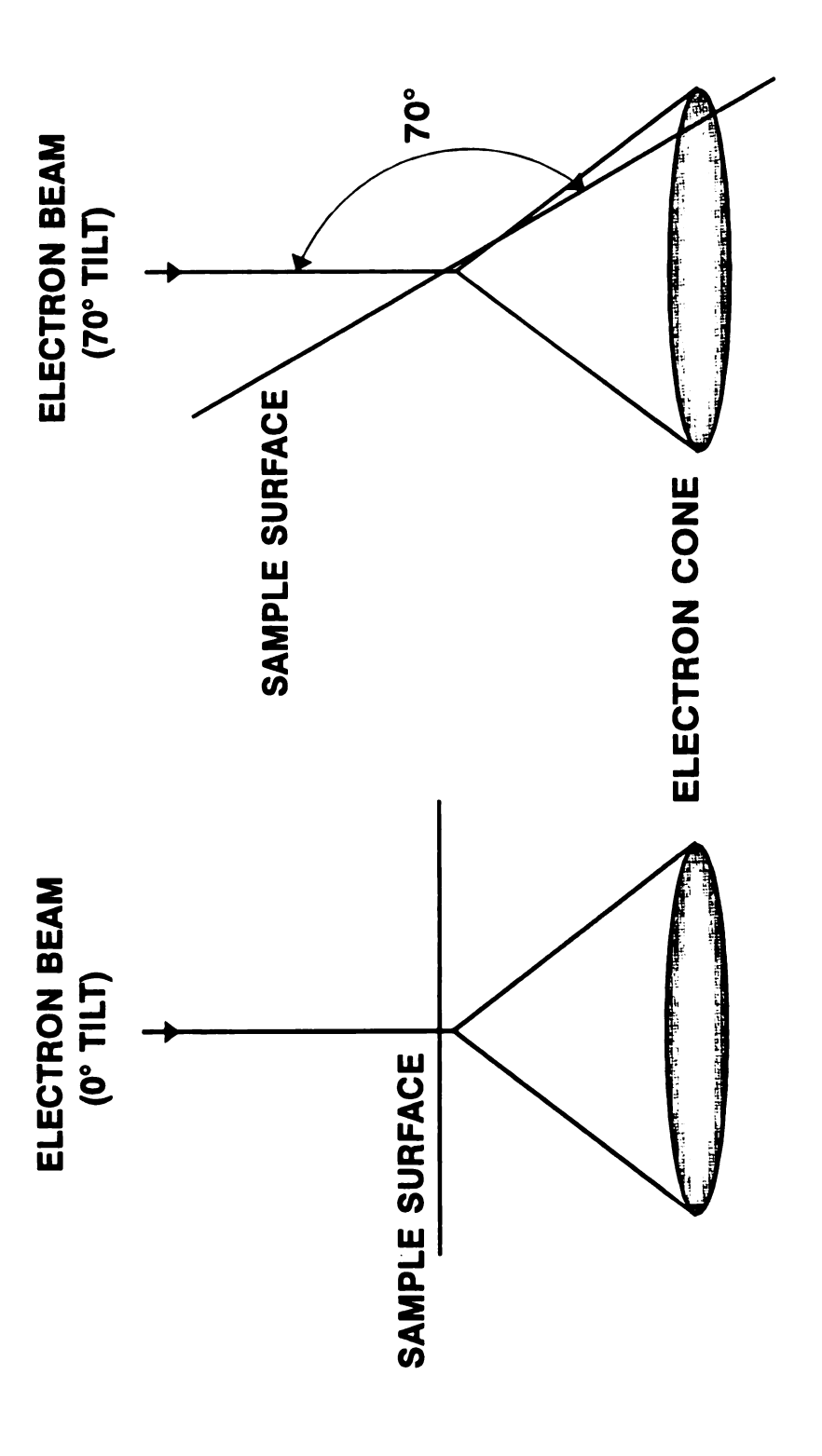


Figure 4

Schematic illustrating the increase in backscattered electrons due to tilting the specimen with respect to the incident electron beam. Adapted from [3].

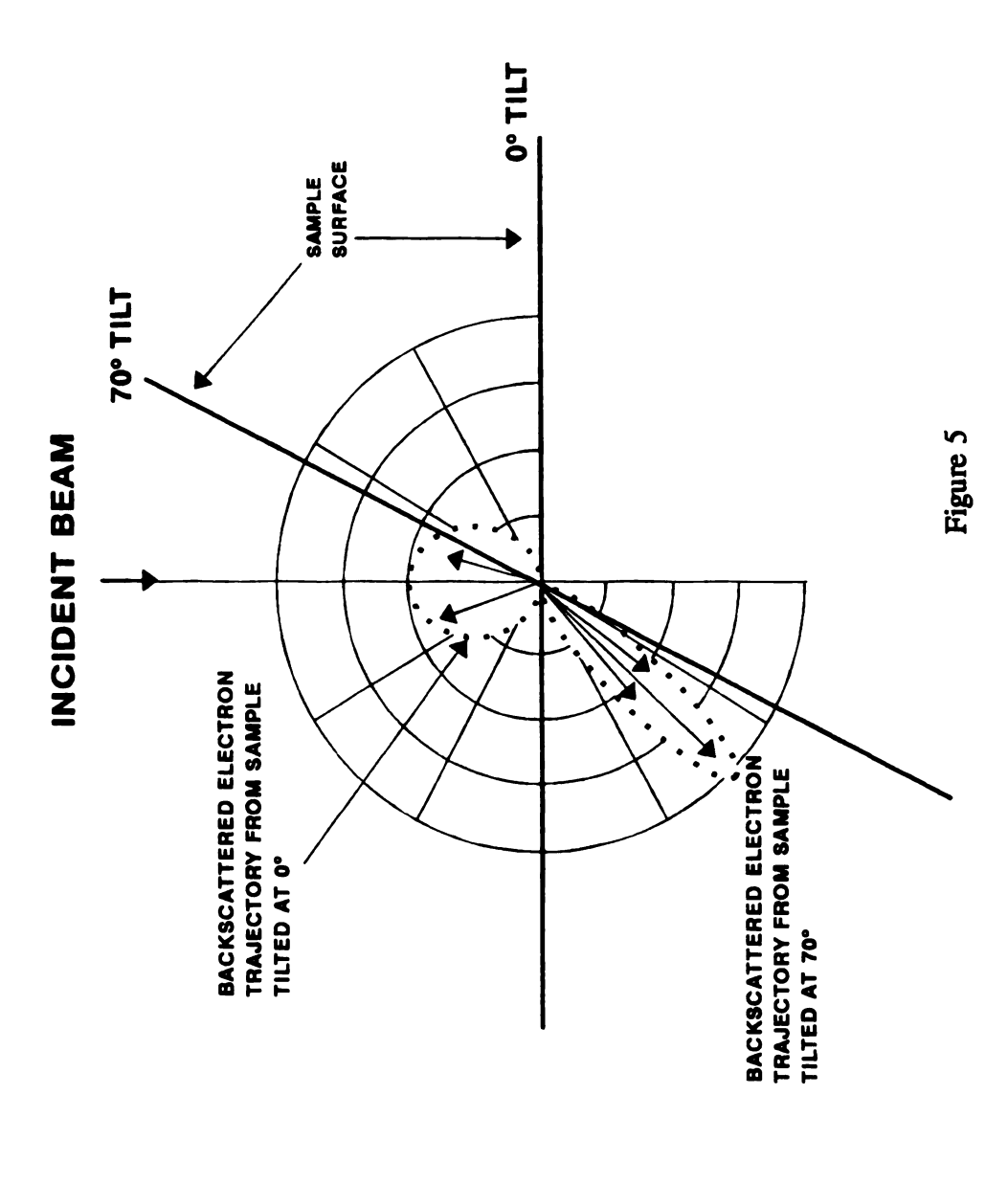


Diagram illustrating backscattered electron trajectories produced when an electron beam is incident normal to a specimen and to a specimen tilted at 70°. Adapted from [3].

a 0° tilt. This is used to experimental advantage in this current study and will be mentioned in the Experimental Procedure and Discussion.

While these backscattered electrons may be used to image the sample, much as with secondary and Auger electrons, via a solid state backscatter electron detector [7], they may also be used to analyze the material in a unique manner through their formation of distinct patterns.

## **Electron Backscattering Patterns**

The distinct patterns, formed by backscattered electrons in the SEM, are referred to by many names. Alam et al. [8] referred to them as "high-angle Kikuchi lines" due to their existence at high scattering angles. More recently, Adams et al. [9] referred to them as BKD patterns, after Backscattered Kikuchi Diffraction patterns. However, the author feels it most appropriate to refer to the patterns as EBSPs (electron backscattering patterns), as referred to in most literature and in the pioneering efforts of Venables and Harland [10].

The formation of these distinct patterns, EBSPs, is still not completely understood, but is geometrically similar to the formation of Kikuchi lines in a TEM. Described in excellent detail by Heimendahl [11], the formation of Kikuchi lines is reasonably straightforward. The incident primary beam electrons are inelastically scattered in all directions in the sample. These inelastically scattered electrons may be further elastically Bragg reflected when conditions are appropriate. Even though this "inelastic" scattering seems to invalidate the very definition of a backscattered electron, they are still referred to as such. Heimendahl further states that 3 crucial facts must be considered:

- (1) Each set of lattice planes produces a line, not a spot. This is due to the fact that the planes are being bombarded by inelastically scattered electrons from all directions. This, of course, is caused by their previously being scattered in all directions. [Note: Since a crystallographic plane is being bombarded from all directions, and all of the electrons satisfying Bragg conditions must meet the same Bragg angle suitable for diffraction for a given (hkl) plane, the exiting electrons actually form a conical pattern [12]. Since  $\theta$ , in Figure 6 below, is so small, the resulting cone has an extremely large circumference where it intersects an imaging medium. The cone is so large that the hyperbola segments seen when intersecting an imaging medium, such as photographic film, may appear as straight lines.]
- (2) The intensity of the initial inelastically scattered electrons decreases with increasing scattering angle. As shown in Figure 6, the electrons scattered at collision B are scattered through a much larger angle (away from the forward direction of the beam) than at A in order so satisfy the Bragg condition at lattice plane (hkl). The collisions at B are not as glancing as at A resulting in a greater transfer of energy away from the impinging electrons. Therefore, they have lost more energy than the electrons from collision A. Therefore, I(A) > I(B).
- (3) Lastly, each plane, positioned nearly parallel with the primary beam, is irradiated from both sides and from all directions as explained above and shown in Figure 6.

These 3 facts, taken together, explain the formation of Kikuchi lines, and for the most part, the formation of EBSPs. Figure 7, more accurately depicting the formation of EBSPs, shows the backscattered electrons exiting the same surface as

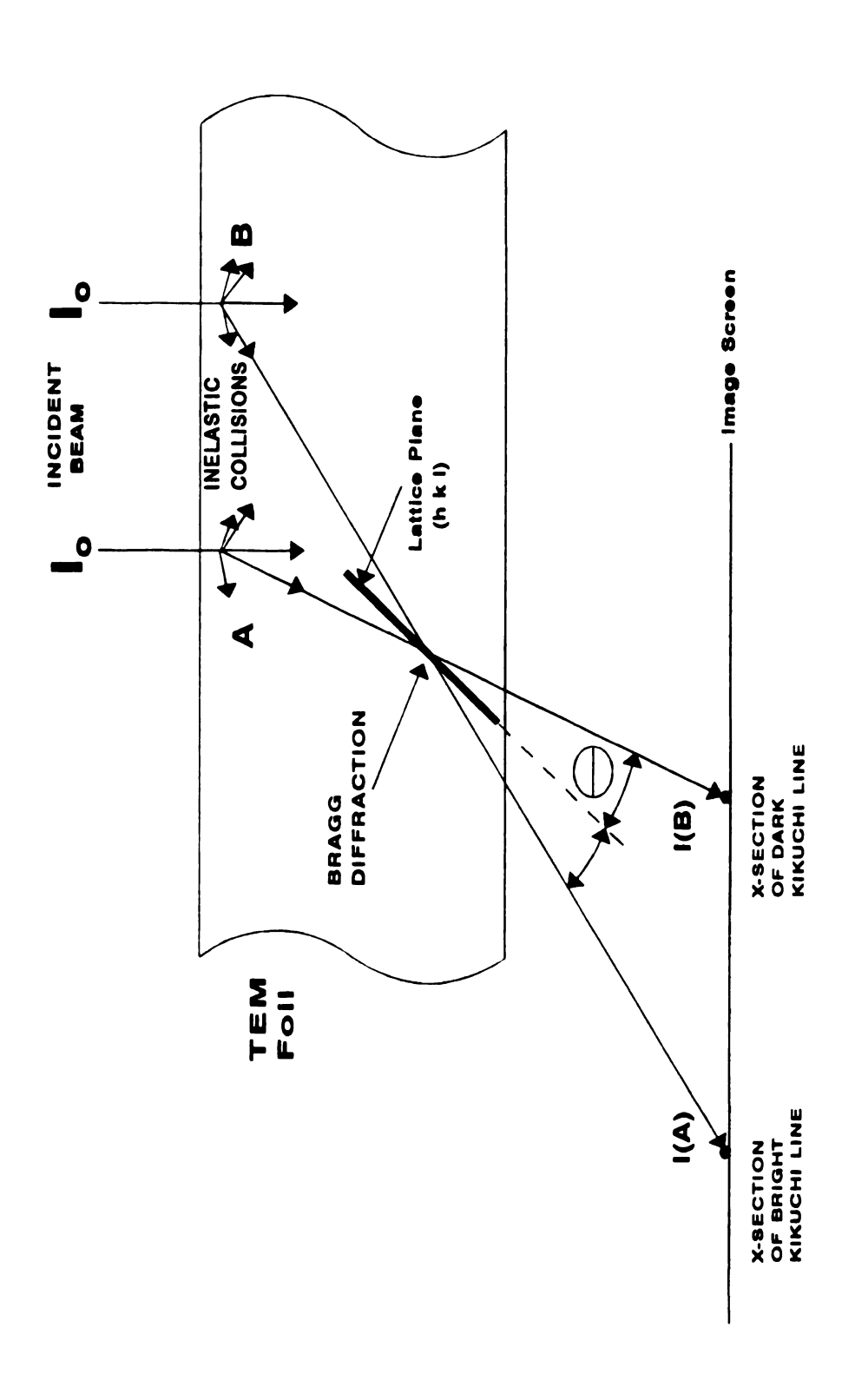
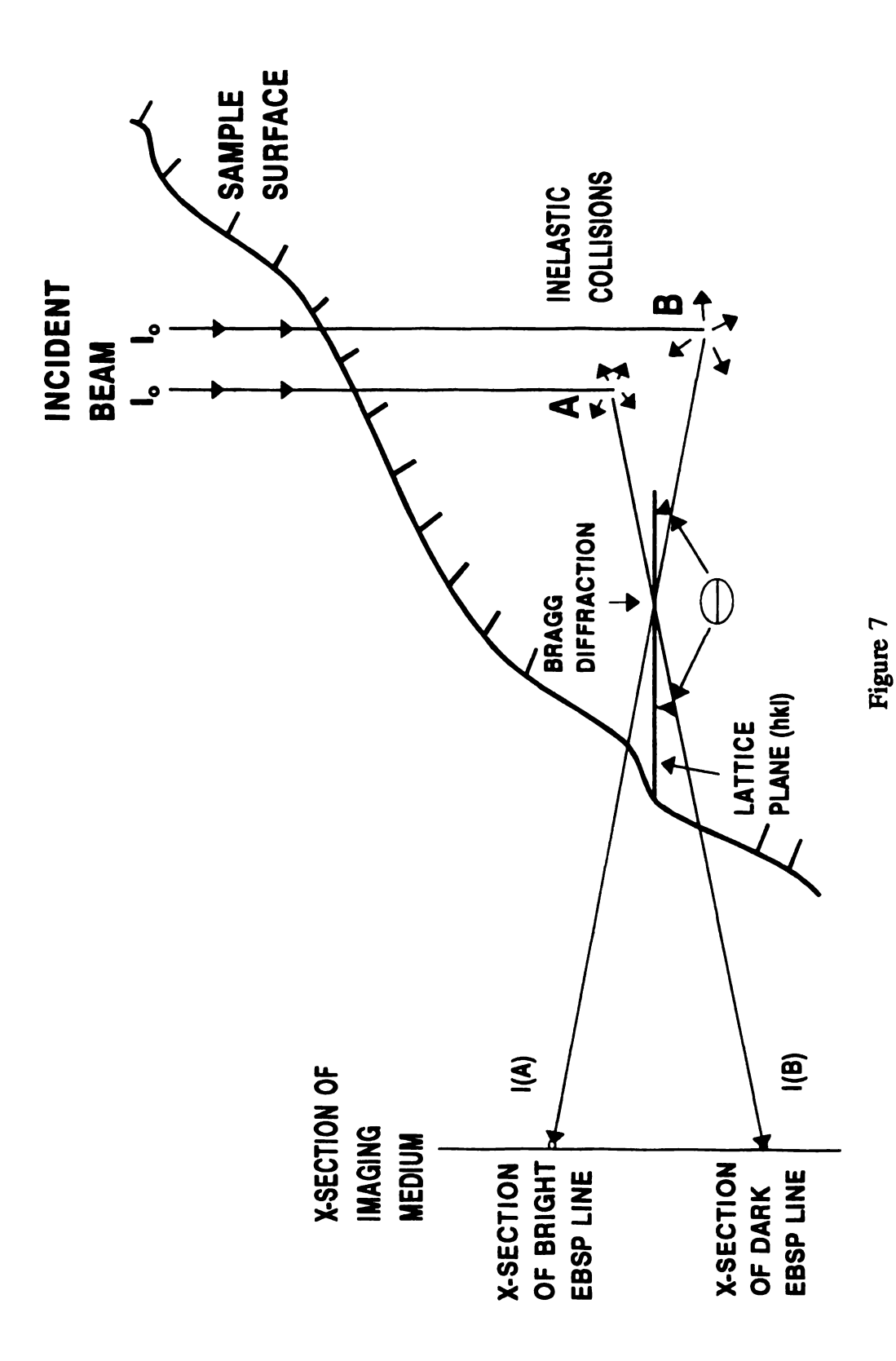


Figure 6

Schematic illustrating the inelastic collisions, Bragg diffraction, and resultant formation and imaging of Kikuchi lines as a result of an incident electron beam. Adapted from [11].



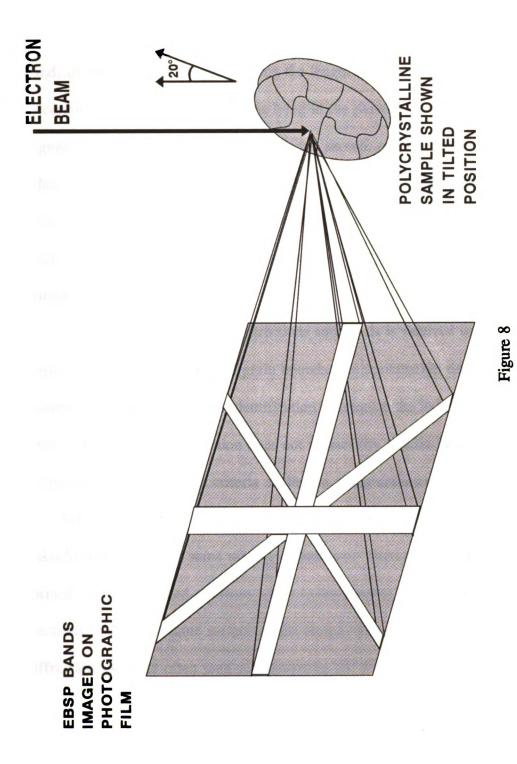
Schematic illustrating the inelastic collisions, Bragg diffraction, and resultant formation and imaging of EBSPs as a result of an incident electron beam.

they entered. The 3 items above, defining Kikuchi lines, also apply to EBSPs. As mentioned in (1) and shown in Figure 6 and 7, the angle  $\theta$  is very small. Using Bragg's Law, Equation 5 states

$$2d_{hkl}\sin\left(\theta_{hkl}\right)=\lambda. \tag{5}$$

Assuming 30 keV electrons of wavelength ( $\lambda = 7.10^{-2}$  Å) incident on (hkl) planes of atomic spacing (d) of a few Å, the resulting angles are in the neighborhood of a few degrees. Thus, it is clear why  $\theta$  is small and consequently why the resulting backscatter cones are large.

In Figure 6 and 7, the lines formed by I(A), having greater intensity, appear bright as compared to the background intensity and are referred to as 'excess' lines. The lines formed by I(B), having lower intensity, appear dark as compared to the background intensity and are referred to as 'defect' lines. In other words, EBSP bands are bound by a dark and bright edge. Figure 8 depicts the formation of the EBSP bands, on a macroscopic level, and their intersection with an imaging medium (perhaps a piece of photographic film), producing the characteristic bands referred to as EBSPs. Note that for EBSPs, similar to Kikuchi lines, two diffraction cones (though not shown) are produced for each set of crystal planes [13]. Since the planes are being bombarded from all sides, one cone is produced from diffraction from the upper side and another cone from the lower side of the planes [14]. Thus, since a divergent source of electrons is bombarding atomic planes from all directions, an



The formation of EBSP bands, on a macroscopic level, resulting from an electron beam incident upon a tilted specimen, and their intersection with an imaging medium. Adapted from [15].

array of diffraction cones is produced characteristic of the planes in which Bragg conditions are satisfied.

A specific set of planes yields a given backscattered electron cone which forms a band, or EBSP, when imaged. Along the length of this band are points corresponding to certain crystallographic directions lying in the parent plane of atoms, as shown in Figure 9. Although all of the bands are not shown, other bands are present from other sets of planes that also contain corresponding crystallographic directions. Bands from different sets of planes which intersect one another at a common point are referred to as zone patterns and correspond with crystallographic zone axes of the sample material.

The determination of these directions and bands is referred to as "indexing".

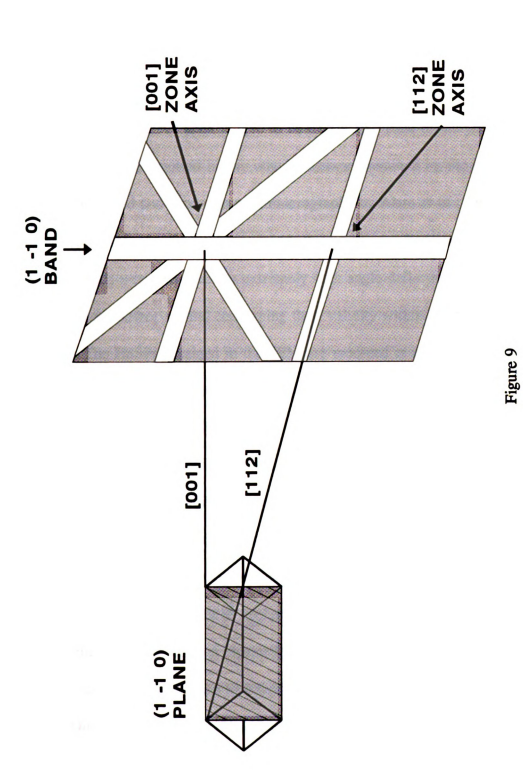
Generally speaking, texture and grain boundary misorientation determination,

orientation imaging and phase identification all require the indexing of EBSPs, while

strain/deformation determination does not necessarily require this indexing. Band

delineation is the important criteria studied in strain/deformation investigations.

While stated that electron backscattering patterns are geometrically similar to Kikuchi lines, there are some notable differences. First of all, Kikuchi lines are formed from transmitted electrons while backscattering patterns are formed from electrons leaving the same surface of the sample that they enter. Also, in the TEM, diffraction spots are often seen accompanying the Kikuchi Lines. This is not seen in the SEM during the formation of EBSPs due to a lack of lenses needed to focus the electrons after leaving the sample. The edges of the bands, one darker and one brighter than the surrounding background, actually coincide with the positions of the



The formation and imaging of EBSPs as a result of backscattered electrons diffracting from a (1 -1 0) plane and the correspondence of the [0 0 1] and [1 1 2] directions with locations on the EBSP. Adapted from [15].

expected Kikuchi lines. Alam et al. [8] state that the bands, similar to the TEM Kikuchi lines, can appear brighter or darker as compared to the background intensity and are also referred to as 'excess' and 'defect' bands. Alam et al. continue to state that the 'excess' bands have been measured to be such by photometric means while the 'defect' lines have been judged to be darker by visual means only. No defect bands have been reported in any other literature examined by the author. The defect bands, reported and shown in photomicrographs by Alam et al., may be the result of their non-SEM experimental set-up, which is explained in more detail later. These defect bands were only seen at extremely high angle deflections. This leaves some doubt in the author's mind concerning their validity within the realm of SEM-related study. The EBSPs obtained in the SEM are recorded at low take-off angles due to their higher intensity, as previously explained.

## 1.2 How and why are EBSPs used

Electron Backscattering Patterns have exceptional spatial and angular resolution. Furthermore, the relatively easy sample preparation necessary to obtain patterns combined with the ease of experimentally obtaining patterns and crystallographic information has led to the increasing use of EBSPs in materials studies. These benefits have proven the EBSP technique to be superior to other diffraction-related techniques, such as electron channelling patterns (ECPs) and Kossel X-ray diffraction, as well as other TEM-based techniques, for many applications.

Dingley and Randle [13] and Venables and Harland [10] report the advantages of EBSP over other diffraction techniques. EBSPs have been claimed to have spatial resolutions as small as 200 nanometers, angular resolutions of 1°, and information

depths of 10 nm. The images produced in EBSP diffraction techniques may be viewed live while those from Kossel X-ray techniques may not. Also, the formation of EBSPs is a relatively efficient process where backscatter coefficients range from 0.1 to 0.6 for most materials, whereas characteristic X-ray quanta information used in Kossel diffraction has an efficiency of 10<sup>4</sup>. Sample preparation for EBSP analysis is relatively straight forward. Bulk samples are used and may only require a freshly cleaved fracture surface for pattern formation, whereas sample preparation for the TEM is often quite involved due to requisite thin foils. With EBSP, large regions of the stereographic triangle may be observed whose size is limited only by the detector used, while TEM and ECP techniques are limited by the diffraction process.

Since the formation of EBSPs is directly dependent upon the material's crystallography, various interpretations of the EBSPs can reveal much information related to the crystallography of the sample. The distribution, orientation [15] and delineation of the EBSPs reveals information about the distribution, orientation, and crystallinity of the atomic planes in the sample. Theoretically, the band width is related to the atomic planer spacing, but is too inaccurate to be reliably used.

Texture [16, 17], strain/deformation [18, 19], and grain boundary misorientation [20] may be determined and orientation imaging [9, 21] and phase identification [22] may be accomplished because of their dependence upon the material crystallography.

After Heimendahl (1980), the crystallographic zone present in an EBSP representing the lattice normal indicates the orientation of the atomic volume under the beam. These lattice normal zones may be determined for a number of grains and used to generate pole figures [23]. This type of information is useful is studying

directionality of grains after processing [16, 25], near fractures [25], and during recrystallization [26]. EBSPs are also useful in the study of grain boundary misorientations. Randle et al. [27] used EBSPs to study the grain misorientation of Ni-based superalloys, concluding that the grain misorientation texture was influenced by grain size. Lee et al. [20] conducted a study of the misorientation texture of post-recrystallized  $\alpha$ -brass. This work also included studying the change of misorientation texture as a function of annealing temperature.

Orientation imaging is an emerging new technology in which EBSPs are used to determine lattice orientations [9, 28, 29, 30]. The EBSP determined lattice orientations are used to construct "orientation images", or maps, of the grain structure. The orientations of the grains are indicated by assigning different colors to the grains and the misorientations between grains are indicated by different grain boundary thicknesses.

Phase identification may be accomplished by indexing an EBSP obtained from an unknown material and comparing it with a list of possible candidates [22, 31, 32].

Many studies of plastic strain/deformation have been conducted using EBSPs.

Wilkinson and Dingley [19] used EBSPs to study the distribution of plastic strain in an MMC that had been strained in tension transverse to the fiber direction.

Unfavorable comparisons of the results were made with those obtained using finite element analysis. Wilkinson and Dingley [33] and Wilkinson [34] have made attempts to quantify plastic strain by studying the degradation of EBSP quality after straining the material in tension. Other attempts to quantify EBSP pattern degradation/quality have been made by Quested et al. [25] at a fracture surface caused

by straining in tension. Wolf and Hunsperger [35] attempted to measure pattern degradation of a GaAs sample after bombardment by 60 keV cadmium ions.

EBSPs may be used to study strain/deformation in a sample due to their relationship with a material's crystallinity. Quested et al. [25] discuss how the delineation of the bands is dependent upon crystal perfection and therefore can yield localized information on dislocation densities. Within the volume of interaction, crystalline perfection necessary to form EBSPs with sharp edged bands is not present. Dislocations and other defects, such as stacking faults and point defects, are responsible for causing local bending of the lattice planes. Therefore, some electrons are scattered away from this perfect Bragg condition causing diffuse edges on the bands [19].

It should be noted that in crystalline materials, measurable strains occur as a result of motion of dislocations. Only those dislocations which move account for strain. Dislocations may be present which do not move, and therefore, do not account for any strain. However, due to the physical nature of backscattering, EBSPs characterize all the dislocations, mobile or immobile, within the interaction volume. Furthermore, EBSPs do not account for plastic strain associated with dislocations which have left the volume of interaction, nor does it account for other recovery processes. This must be considered when using EBSPs to represent strain [36].

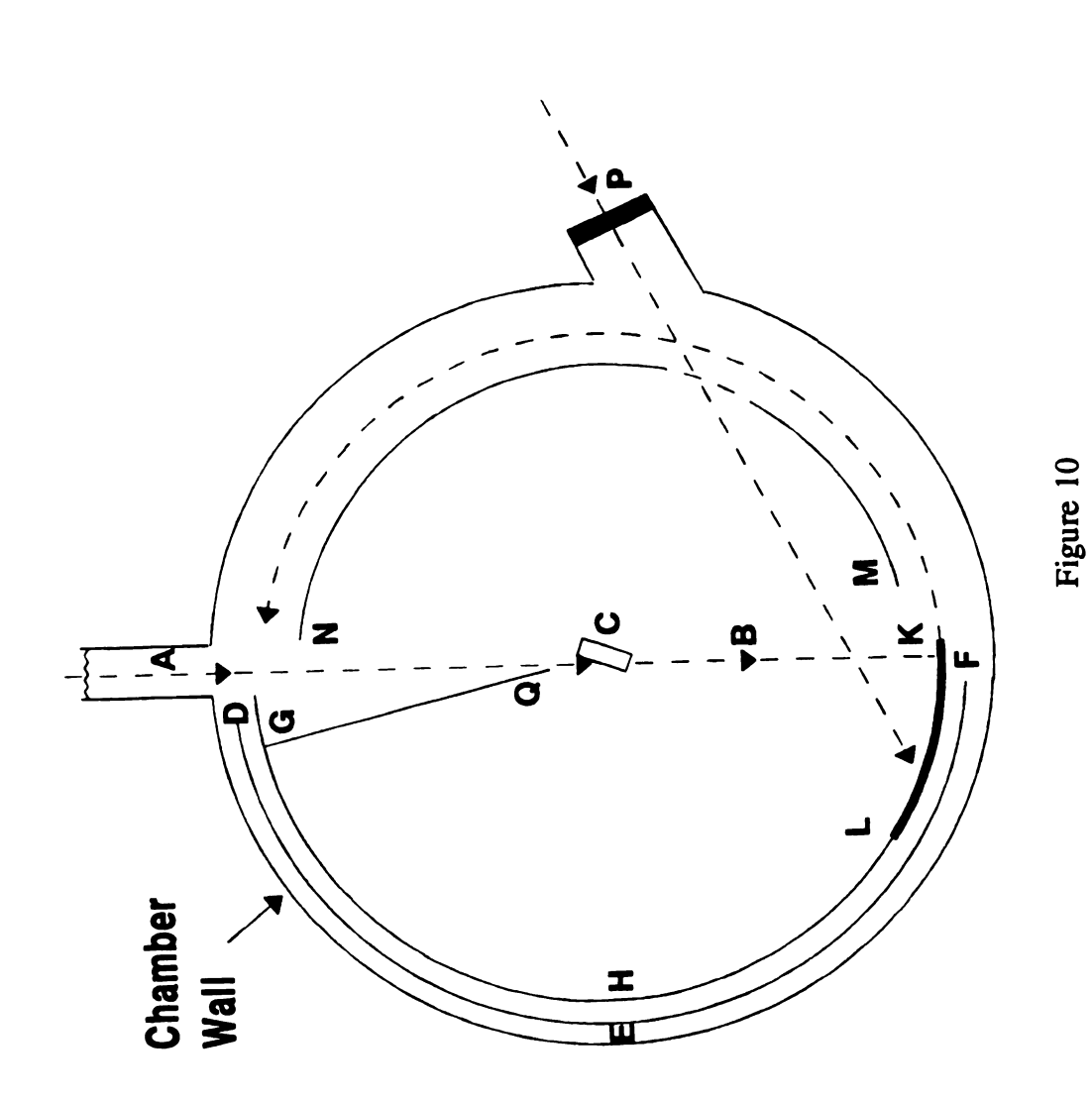
Summarizing, when a material is strained by a physical or chemical process, thereby introducing dislocations into the crystalline lattice, diffuseness is also introduced into the EBSP bands [19, 33, 35].

#### 1.3 EBSP recording systems

One of the first published instances of researchers recording electron backscattering patterns was by Alam et al. [8]. Instead of using an SEM, Alam used a specially constructed flat, cylindrical chamber shown in Figure 10. The incoming beam, direction AB, struck the specimen at C. A piece of photographic film, DEF, was mounted in a cylindrical frame and recorded EBSPs through a range of 164°. A metal cover, GHK, protected the film from electron exposure until it was rotated about the cylinder axis to expose the film. Through trial and error, Adam et al. noticed that while partially uncovering the film to record limited EBSP angles, electrons that struck the metal cover scattered onto the film and caused a background fogging. Of course, this fogging was a result of the very same backscattered and secondary electrons mentioned earlier. A metal shield, GQ, blocked the unwanted scattered electrons from striking the film. An additional shield, NM, prevented any afterglow from the fluorescent screen LK from causing background fogging. Interestingly, their setup allowed for the viewing of the fluorescent screen through port P.

In 1973, some 19 years after the work of Alam et al. [8], Venables and Harland [10] reported obtaining EBSPs in an SEM and used them to investigate microcrystallographic information. Venables and Harland also imaged the EBSPs with a fluorescent screen. The screen was viewed in transmission by a closed circuit TV camera. In order to get hard copies of the images, a 35mm camera, mounted outside the SEM chamber, was used to take photographs of the TV screen.

Subsequently, several researchers used the fluorescent screen/TV camera set-up



Cylindrical chamber used, in one of the first published instances, to record electron backscattering patterns. Adapted from [8].

to view the EBSPs but obtained hard copies of the images by using photographic film placed within the SEM chamber [19, 33, 37]. In some cases, film transfer devices were fabricated while in others, the recording systems consisted of a means to hold a single piece of photographic film in place within the SEM chamber [2, 38, 39]. In some of these systems, only one EBSP could be recorded at a time before the vacuum needed to be breached in order to change the film [22]. These film transferring and exposure problems are noted by Michael and Goehner [22].

Other advancements were noted by Dingley and Baba-Kishi [31] when they viewed the EBSPs using the fluorescent screen/TV camera set-up interfaced with a computer to facilitate on-line analysis of the patterns. However, superior quality EBSPs were recorded using the photographic film technique of Wilkinson and Dingley [19, 33].

More recent advances in improving pattern imaging quality involve the use of charge coupled device (CCD) based detectors. Michael and Goehner [22] used a single crystal scintillator to image the EBSPs. The scintillator was coupled to a CCD via a fiber optic cable. The CCD and scintillator were bonded directly to the fiber optic with a thin layer of transmissive epoxy, thus reducing any signal loss and additional light noise. The quality of the resulting raw images does not justify the use of the CCD over recording with photographic film. However, the CCD was interfaced with a computer for image processing and analysis. The image processed EBSPs demonstrated high quality.

The orientation imaging developed by Adams et al. [9] does not require hard printing of the EBSP since their system incorporates on-line analysis. However, the

digital image needs to be of sufficient quality for computer image recognition. Many of the systems currently being used [9, 23] have built-in image processing mechanisms incorporated with pattern recognition programs and automatic indexing and texture determination arrangements. Nevertheless, recording directly on film yields outstanding quality and detail; in some cases beyond that of standard image processing techniques [40]. A much more detailed examination of image processing systems including transforms and pattern recognition programs is given by Balcers [41], Lassen et al. [42], and Wright and Adams [43].

Actual EBSP sample/imaging device geometric considerations are well developed. Alam et al. [8] noted early on that higher glancing angles yield better band-to-background signal contrasts. Background signals include backscattered electrons not involved with above described Bragg diffraction as well as Auger electrons and secondary electron signals from a variety of sources. Flegler et al. [2] describe four sources of secondary electrons. Secondary electrons may be produced directly from the beam-sample interaction, by backscattered electrons as they exit the sample, by backscattered electron-SEM chamber interactions, and by electron beam-aperture interactions. All of these secondary electrons may contribute to the background signal.

Along with better band-to-background contrasts, Alam et al. [8] noted that higher glancing angles yield larger backscatter electron signals. Venables and Harland [10] and Dingley [37] credited Alam et al. for this discovery and also conducted their EBSP experiments using angles of incidence between 70° and 80°. Larger angles of incidence, although yielding higher backscatter coefficients,  $\eta_{\rm RSE}$ ,

result in lower penetration depths. EBSPs have the advantage of yielding information from a given volume at certain depths below the surface.

The EBSP technique is not merely a surface tool, but may become one when tilts exceed approximately above 70°. Larger angles of incidence (> 75°) also produce an extremely large fraction of secondary electrons contributing to background signal, thus reducing band-to-background contrast. Goldstein *et al.* [3] report asymptotic behavior near 80° with the secondary electron coefficient going to infinity. Additionally, Dingley [37] reports that higher angles of incidence near 85° result in excessive probe elongation in the interaction volume causing diffuse patterns. Furthermore, since the interaction volume is effectively enlarged in the surface plane, unwanted EBSP diffraction information may be obtained from other grains, dislocation subcells, and phases. These considerations have lead to an incident angle of 70° as the standard for most EBSP studies.

When using the EBSP technique, the SEM is used in spot mode as opposed to raster mode [37]. It is also necessary to carefully focus the beam while in secondary electron imaging mode prior to switching to spot mode [33]. These practices, like the above EBSP related sub-procedures, are necessary to improve spatial resolution by decreasing the interaction volume, thus decreasing residual electron noise and unwanted diffraction information while, at the same time, increasing the pattern-to-noise ratio. It is ultimately necessary for the beam diameter and interaction volume to be smaller than the crystal from which the EBSPs are obtained. In Dingley's 1984 publication [37], achieving distinguishable patterns from 2  $\mu$ m grains was possible, though inconvenient. Further reductions in beam current, corresponding to a probe

diameter of 10 nm, resulted in distinguishable patterns, but only after 15 minutes of exposure. In 1992, Dingley and Randle [13] reported a spatial resolution of 200 nm.

#### 1.4 Sample Preparation

Dingley and Randle [13] state that there are two essential prerequisites for obtaining EBSPs. The first, ensuring a sample tilt angle of 70° from horizontal, has already been discussed. The second requirement relates to obtaining a relatively strain free, clean surface suitable for the EBSP technique.

#### Strain/deformation

"Strain free" does not mean free of all and any strain in the material. Obviously, as mentioned earlier, studying strain/deformation in a material is one important aspect for which EBSPs are very well suited. The strain that needs to be avoided, in this case, is the artifact strain induced on and near the surface of the material as a result of mishandling or sample preparation procedures. In softer materials, mechanical polishing, while removing deformed material, also introduces damage, or plastic deformation. For example, an annealed polycrystalline 70:30 brass sample abraded on 220-grit SiO<sub>2</sub> paper can exhibit induced deformation as deep as 10 µm [44]. Indeed, Harland et al. [45] report that EBSP diffraction information is obtained from within 10 nm of the surface (albeit using a field emission SEM). Another analysis shows that at 30 keV, backscattering patterns disappear after applying a 10 nm coating of aluminum while at 20 keV, the patterns become invisible after applying a 5 nm coating [37]. This implies the patterns originate from the top 10 nm of material [37]. Thus, it becomes obvious that the near-surface volume of the material needs to be free of artifact plastic deformation. The removal of this

deformed layer may be facilitated by several means. Electropolishing (discussed below), etching, acid string saw cutting, EDM, and ion milling may all be used to this end. However, electropolishing is more commonly used when preparing EBSP samples due to its relative ease, low expense, and wide expanse of reference material [11, 46, 47]. Additionally, archaic yet effective electropolishing cells are easily fabricated with inexpensive materials and components.

#### Surface cleanliness and smoothness

Surface cleanliness may be achieved by several methods. The production of a fresh fracture surface by methods such as cleaving a brittle material, ultrasonic cleaning in either water or a solvent, electropolishing, ion milling, and acid string cutting have all been used to produce a clean surface. Surface contamination occurring within the SEM chamber can have detrimental effects on EBSP analysis by reducing the quality of the pattern, thus possibly giving erroneous indications of strains. Wilkinson and Dingley [19] state that in order to avoid these surface contamination problems, the sample should only be observed for a few seconds at high magnification before switching to spot mode to obtain an EBSP. Not only does the secondary electron image darken due to surface hydrocarbon contamination, but the resulting EBSP pattern quality deteriorates with increasing beam exposure time. Wilkinson and Dingley [33] state that a 1 minute scanning mode beam exposure over a 40  $\mu$ m x 40  $\mu$ m area at 5000X will produce the equivalent pattern degradation of a 1% strain.

Yet another important prerequisite for producing surfaces that yield high quality EBSPs lies in the understanding of surface smoothness. The sample surface needs to

be smooth on the order of the beam diameter so that chaotic surface diffraction does not occur. Fortunately, locating areas that are flat on the order of the beam diameter is relatively easy even in macroscopically rough specimens [31]. Alternately, macroscopically smooth surfaces can often look impressive, but be deceivingly rough on the microscopic scale. Surface smoothness can best be achieved by proper electropolishing techniques.

#### **Electropolishing**

While the exact mechanisms of electropolishing are still not completely understood, this approach still has the ability of removing all traces of deformation induced by mechanical polishing operations in sample preparation. Electropolishing is also used to remove surface imperfections and oxides. Most metal alloys have a fine, thin, surface oxide layer present under normal equilibrium. Davidson [36] states that under good conditions, these oxides are easily penetrated by electrons and may normally be considered unimportant. In order to achieve these "good" conditions, metals are often electropolished, thus ensuring a thin, uniform oxide layer. Electropolishing is used to prepare samples for observation in optical, scanning electron, and transmission electron microscopy.

As explained in Metals Handbook [47], electropolishing is thought to include both a smoothing action and a brightening action. The smoothing action is accomplished by preferential attack of hills and ridges on the surface commonly produced by mechanical polishing. When the surface is made the anode in an electropolishing cell, a viscous polishing film forms on the surface of the sample and acts as a resistance layer. The hills lying closer to the edge of this resistance layer,

have lower resistance than the valleys, and therefore have a higher current. This higher current causes the hills to dissolve much faster than the valleys resulting in a smoothing action.

The brightening action is a result of the removal of surface irregularities on the order of 0.01  $\mu$ m. Etching, a common occurrence in stages of electropolishing, must also be avoided in order to achieve this bright surface if so desired.

Electropolishing results from a simple relationship between current and voltage that is sometimes difficult to control. It is important to note, however, that the voltage is the quantity primarily affecting the polishing conditions, while the current is a variable depending on sample size [11]. Figure 11 schematically represents this relationship for the electropolishing of aluminum in a perchloric acid (HClO<sub>4</sub>) electrolyte. At lower voltages, a passivating film forms on the surface preventing the passage of current. This scenario is similar to placing the sample in a chemical etchant. Indeed, etching does occur under these conditions of low current/voltage. However, it is seen that electropolishing occurs over a continuous range above some critical voltage level. Above this level, the passivating film is broken allowing current to pass through to the sample affecting an ionic exchange between metal and electrolyte. A much more complex current-voltage relationship is illustrated in Figure 12. Here, etching occurs in the region between AB where no current passes. Electropolishing occurs in the region BC characterized by a constant current density with increasing voltage. Region CD often reveals its character by causing pitting on the sample. This pitting is due to gas bubbles breaking the polishing film surface causing momentary, localized increases in current.

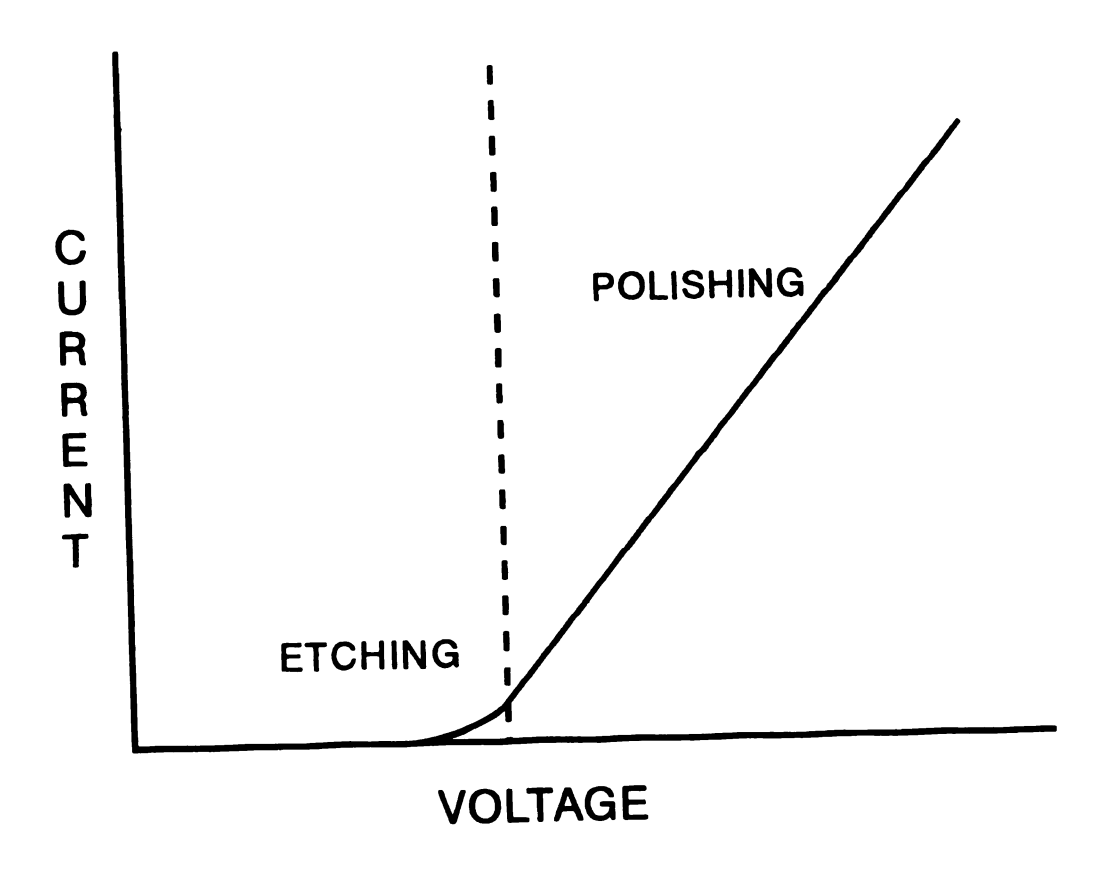


Figure 11

Current as a function of voltage representative of the relationship seen when electropolishing aluminum in perchloric acid based electrolytes.

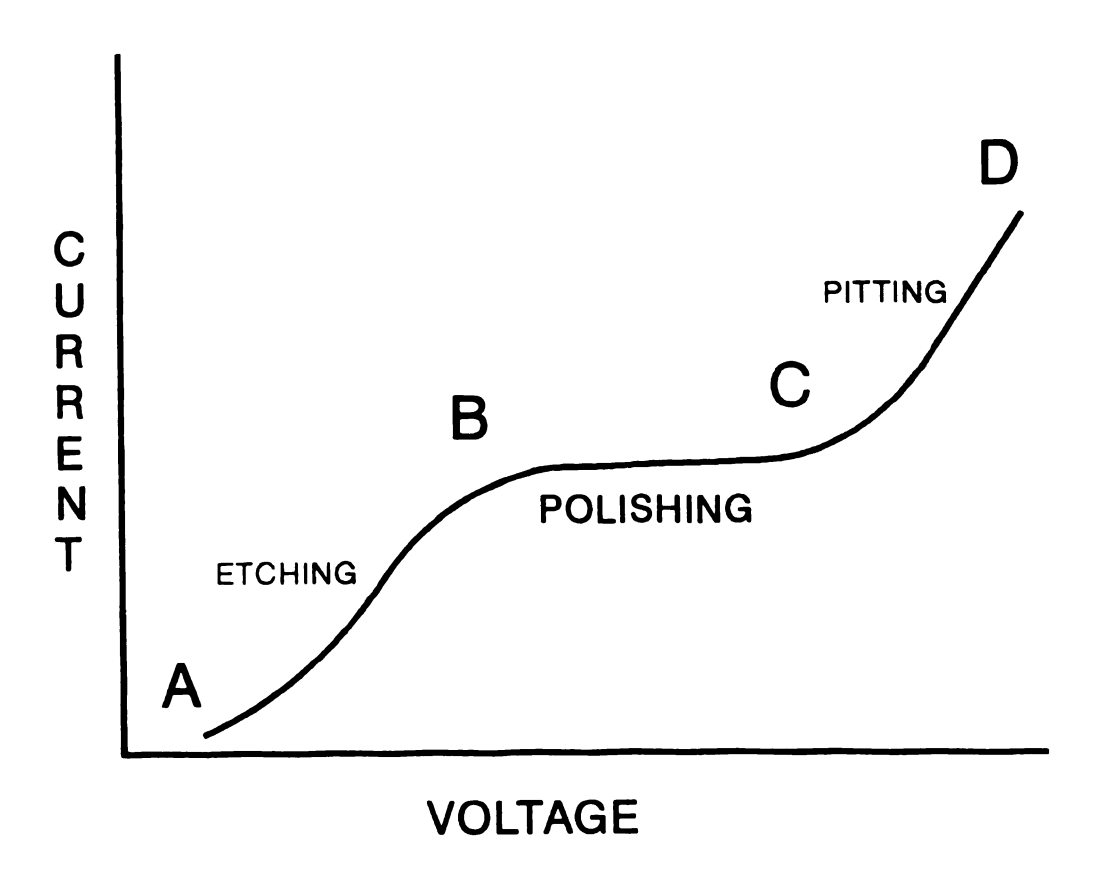


Figure 12

Current as a function of voltage representative of the more complex relationship seen when the potential exists for etching, polishing, and pitting.

In order to properly electropolish a specimen, only the surface for which electropolishing is desired should be in contact with the electrolyte. Many times, this can be accomplished by mounting the specimen in a mounting compound. However, some mounting compounds may react violently with the electrolyte. For example, Bakelite should not be used when electropolishing in perchloric acid compounds due to explosion hazards. Perchloric acid has a brief but violent history of explosion hazard [48]. A chemically inert, insulating lacquer is often used to paint the areas where electropolishing is unwanted.

After Metals Handbook [47], electropolishing cells usually consist of a current source, usually DC, with some means of varying the potential. The cell also consists of a container for the electrolyte often surrounded by some type of cooling mechanism. Lower temperatures result in a slower, more controlled polishing process [11] as well as present safer conditions for electrolytes to function [48]. Another advantage of using lower temperatures lies in the expanding of the current-voltage plateau, discussed later [46]. A stainless steel beaker is often used as the container as it can act as the cathode as well as being impervious and inert to most electrolytes. Also, the cell often contains a means for stirring either the electrolyte or the specimen during polishing to help remove any chemical by-products from the specimen surface that might interfere with the electropolishing process. Ideally, the stirring should be nondirectional to prevent furrowing on the surface. But these macroscopic irregularities are often insignificant in EBSP analysis, as stated earlier.

Prior to placing the specimen in the electropolishing cell, it is a good idea to pre-clean the sample. Aluminum alloys can be precleaned in a 5% NaOH solution for

30 seconds in order to remove any surface contamination, dirt, or finger oil that might detrimentally affect the local electropolishing rates [49].

The specimen is made the anode and placed in the cell so that the surface to be polished faces the cathode. Depending on the type of polishing occurring, under passivating film or by gas evolution, the surface is placed either horizontally or vertically. Vertical placement, if at all possible, is best used as it allows bubbles better opportunity to escape from the surface thereby decreasing the chance for pitting.

Experimental settings rarely produce the ideal current-voltage relationship shown above in Figure 12. Electropolishing curves rarely show this perfect plateau. However, there is usually an area on the curve where the slope falls off somewhat giving the researcher an indication of where to begin electropolishing. Lower temperatures, as already stated, aid in expanding this plateau. After an initial test, some minor adjustments may bring the cell to its optimum setting. These electropolishing current-voltage curves may be determined experimentally. After the cell is constructed, the voltage is adjusted on the potentiometer and corresponding currents are recorded. Plotting these data points may reveal the necessary plateau needed to obtain optimum electropolishing although some researches have had little success with this technique [50, 51].

As stated above, electropolishing is used to prepare samples for EBSP analysis in order to remove irregularities, oxides, and surface deformation artifacts often introduced during mechanical polishing. Indeed, most published research briefly states the manner in which the sample was prepared.

An aluminum MMC consisting of 140 µm diameter silicon carbide fibers can be successfully prepared by mechanical polishing, followed by electropolishing with a 10% nitric acid in ethanol solution [19]. This electropolishing should be done, at the very least, the same day as the EBSP analysis to reduce excessive and uneven oxide build-up. A commercially pure 1100 aluminum alloy can be prepared for EBSP analysis by mechanically polishing down to 5  $\mu$ m aluminum suspension followed by a 30% nitric acid in methanol electropolish and an etchant to reveal grain boundaries [21]. Bottcher et al. [16] sputtered the prepared surfaces of cold rolled electrical steel with neutral argon atoms in order to provide an accurately flat specimen. Dingley and Baba-Kishi [31] electropolished  $\beta$ -tin with Struers A2-1 electrolyte and kept the sample in solvent until just prior to analysis. Dingley [37] electropolished IN718 superalloy in order to remove the surface work induced by mechanical polishing. Using a technique developed by Davies et al. [52], a series of papers on the penetration depth of ions in tungsten [53], silicon [54], and aluminum [55] describes the conversion of a known thickness of the metal to an oxide. The oxide layer is then dissolved in some aqueous solution to reveal an extremely uniform surface. This technique has been called electrochemical stripping or anodizing-stripping.

Unfortunately, most sample preparation procedures, deemed so critical for EBSP analysis, are unsatisfactorily explained in EBSP publications. This leaves the current researcher repeating studies to determine electropolishing procedures for selected materials.

#### 1.5 Objectives

A prior EBSP related investigation [38] in the MSM department at MSU used a commercial LINK system employing a phosphor screen imaging medium coupled with a low light TV camera. Also, an FeAl alloy of a sufficiently high atomic number was used resulting in average pattern quality. Even though hard prints of the patterns were not required for the texture analysis, a single hard print was made for illustrative purposes, using a piece of electron sensitive film placed in the SEM chamber. Sufficient for this previous study, the LINK Merlin EBSP camera system may not be adequate for other studies using low atomic number elements or studies requiring high quality EBSPs for strain comparisons. Therefore, an alternate recording system, one using a 35mm camera body, was investigated in the present study.

Initially, it was important to see if the 35mm camera body system had the ability to record high quality EBSP images with some appropriate, electron sensitive film.

Additionally, it has been determined if the commercial LINK Merlin EBSP camera system had the ability to successfully yield high quality EBSP images, from relatively low atomic number aluminum alloys. This study describes the development of this 35mm camera body EBSP recording device and compares the results with the output of a commercial LINK Merlin EBSP system. Furthermore, because of the importance of sample preparation on obtaining high quality EBSP images, the effects of electropolishing on EBSP image quality has been examined.

Once the feasibility of using the 35mm camera body system for recording high quality EBSPs had been determined, examinations into its usefulness were conducted.

Therefore, another goal of this study was to discover whether the system could be used to qualify strain in certain aluminum alloys.

#### 2. EXPERIMENTAL PROCEDURE

#### 2.1 Material

The GaAs single crystal material used in this study was supplied by Professor M. Aslam, Department of Electrical Engineering, Michigan State University, in thin wafer, semiconductor, as-polished form, 0.62 millimeters thick.

The commercially pure aluminum in this study was supplied by Dr. D. A.

Grange, ALCOA Technical Center, for a previous study. The material was ingot cast and vacuum remelted and contained equiaxed grains averaging 2mm diameter in its as-received form.

The (Al<sub>2</sub>O<sub>3</sub>)<sub>p</sub>/6061 aluminum material used in this study was supplied by Prof.

K. Subramanian, Department of Materials Science and Mechanics, Michigan State

University. The (Al<sub>2</sub>O<sub>3</sub>)<sub>p</sub>/6061 aluminum material was extruded, solution annealed at

560° C for 1 hour, room aged at 24° C for 65 hours, then artificially aged at 170° C for 14 hours in its as-received form [56].

#### 2.2 Sample Preparation

#### 2.2.1 GaAs

In its supplied form, the GaAs semiconductor wafers were single crystal and polished to a mirror finish. The only additional preparation required prior to acquiring EBSPs was the rinsing of the wafer in methanol prior to analysis.

#### 2.2.2 Commercially pure Al and (Al<sub>2</sub>O<sub>3</sub>)<sub>p</sub>/6061 aluminum

#### **Mechanical Polishing**

The aluminum based materials were cut to an approximate 1.0 cubic centimeter shape using a Buehler Iso-cut<sup>TM</sup> diamond wafering blade mounted in a Struers

Accutom-5<sup>TM</sup> high speed cutoff machine. Grinding on a 180 grit sandbelt was sometimes necessary to ensure that the surface to be studied was parallel to its opposing surface for mounting purposes.

At this point, a 0.080 in. diameter hole was drilled and tapped into the sample face opposite the one to be used in the EBSP analysis. This was so a screw, which would serve as anode lead attachment, could be screwed into the sample without disturbing the material near the analysis surface.

#### **Heat Treatment**

The commercially pure Al was given a full anneal at 450° C for 1 hour and then furnace cooled. This was done to ensure a reasonably strain free, uniform material.

The (Al<sub>2</sub>O<sub>3</sub>)<sub>p</sub>/6061 aluminum alloy was solution annealed at 560° C for 8 hours and then air cooled to eliminate all precipitate phases that might interfere with the EBSP analysis.

#### **Metallographic Preparation**

The surface of interest was then mechanically ground on 240, 320, 400, and 600 grit SiC metallographic papers, respectively. Following which they were polished using 5.0  $\mu$ m, 3.0  $\mu$ m, and 0.5  $\mu$ m alumina lapping solutions, respectively, on billiard polishing cloths.

#### **Electropolishing**

An electrolytic cell was constructed in order to facilitate electropolishing of bulk samples. The potentiometric circuit cell consisted of a DC Struers Polipower<sup>TM</sup> power source potentiostat containing both voltage and current readout meters. The positive (+) lead from the power source was connected to the screw in the sample,

thus making the sample the anode in the cell. All surfaces of the anode, except for that surface to be subjected to EBSP analysis, as well as any parts of the positive lead that would be submersed in the electrolyte, were painted with Microshield<sup>TM</sup> acid resistant lacquer. A stainless steel beaker served as both the electropolishing solution container and cell cathode once the negative (-) lead from the potentiostat had been connected directly to the beaker. The stainless steel beaker was placed in an insulated dry ice/methanol bath maintained at 0° C. This bath was then placed on a Thermolyne Nuova II<sup>TM</sup> magnetic stirring plate so that the electrolyte could be continuously stirred, with a 1" magnetic stirring rod placed directly in the stainless steel beaker (Figure 13). Prior to being introduced to the electropolishing cell, the samples were subjected to 30 seconds of cleaning in a 5% NaOH solution in order to remove any surface contamination that might cause uneven electropolishing. The optimum electropolishing conditions for the commercially pure Al were found to be an electrolyte consisting of 70 ml distilled H<sub>2</sub>O, 350 ml ethanol, 50 ml 2butoxyethanol, and 30 ml H<sub>2</sub>ClO<sub>4</sub> (perchloric acid) maintained at 0° C. The approximate 0.60 sq. cm. surface area was electropolished for times ranging from 5 to 25 minutes (depending on the particular experiment) at 20.0 V resulting in a current of 0.66 mA (i.e. a current density of 1.1 mA/cm<sup>2</sup>). After electropolishing, the commercially pure aluminum sample was etched in a 10% HF(48%)/distilled H<sub>2</sub>O solution for 1 minute, rinsed in running hot tap water, methanol, and blow-dried in hot air. A final 3 minute ultrasonic methanol rinse followed and immediately preceded placing the sample in the SEM.

The optimum electropolishing conditions for the  $(Al_2O_3)_p/6061$  Al were found to

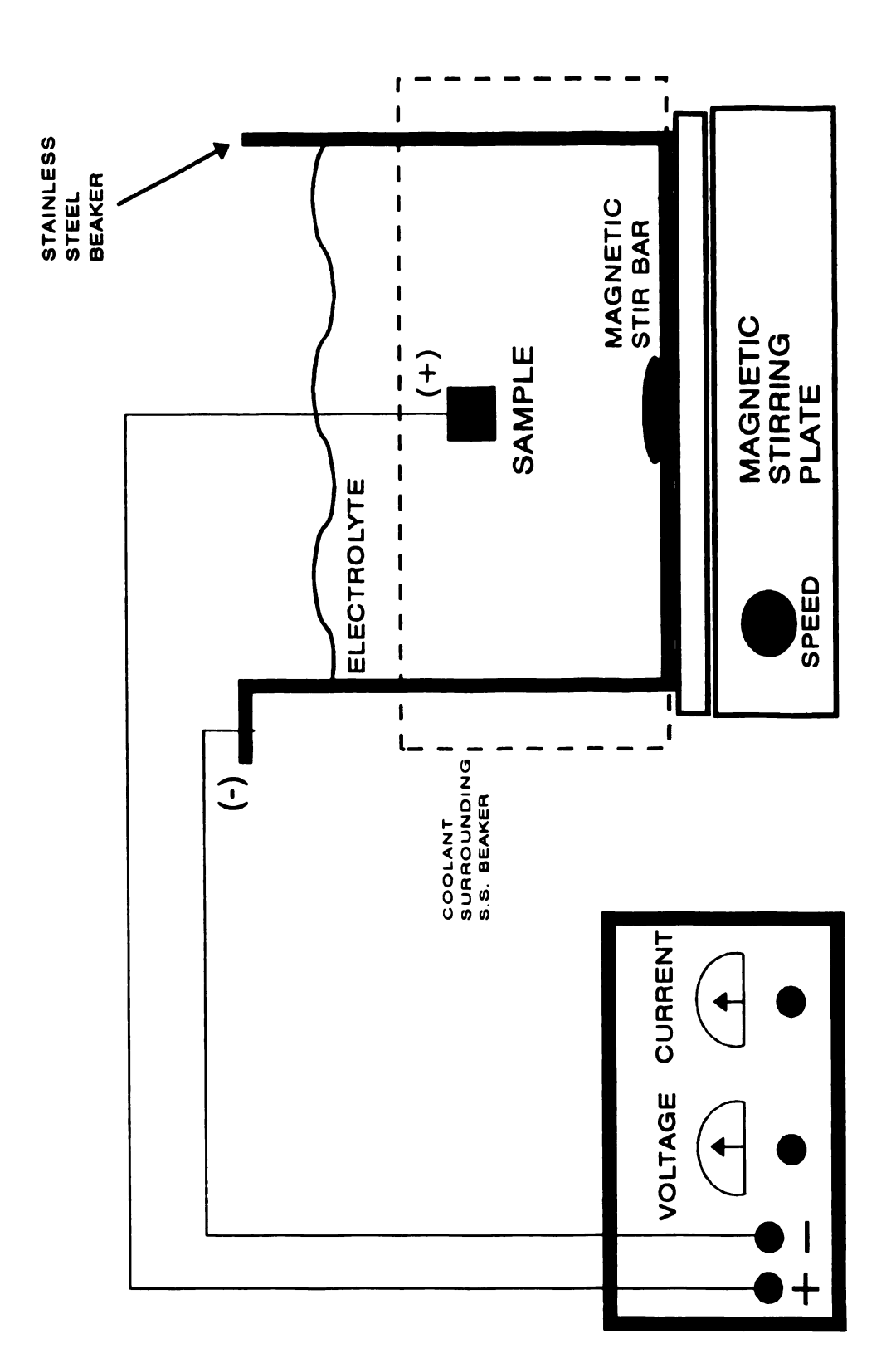


Figure 13

Diagram of electropolishing cell.

be an electrolyte consisting of a 33% HNO<sub>3</sub>/methanol solution maintained at 0° C. The approximate 0.80 sq. cm. surface area was electropolished for 5 minutes at 5.0 V resulting in a current of 0.24 A (i.e. a current density of 0.3 A/cm<sup>2</sup>). After electropolishing, the (Al<sub>2</sub>O<sub>3</sub>)<sub>p</sub>/6061 Al sample was etched in Keller's etch, consisting of 1.0 ml HF(48%), 1.5 ml HCl, 2.5 ml HNO<sub>3</sub> and 95.0 ml H<sub>2</sub>O, for 30 seconds, rinsed in hot tap water, methanol, and blow-dried in hot air. Again, a final 3 minute ultrasonic methanol rinse followed and immediately preceded placing the sample in the SEM.

#### 2.3 Camera Systems

#### 2.3.1 35mm Camera/Sample Set-up

A camera mounting plate was fabricated from aluminum sheet. The mounting plate was attached to pre-existing holes in the side of the specimen stage with camera mounting holes large enough so the camera body position could be fine-tuned in the X and Y directions. The camera body chosen for this work was the Canon EOS Rebel XS<sup>TM</sup> as it was small enough to fit within the confines of the Hitachi S2500 SEM chamber and offered an electronic motor drive which could be conveniently configured as outlined below. The resulting specimen/camera configuration is shown in Figure 14. The specimens were mounted, using 2-sided carbon tape, on a specially designed sample holder that would maintain the sample surface at an angle of 70° from horizontal. The importance of this angle was discussed earlier. The sample surface was located facing the film plane of the camera body. When using the 35mm camera set-up, the area of interest on the specimen surface was positioned so that it lay nearly horizontal with the center of the recording film. A remote electronic cable

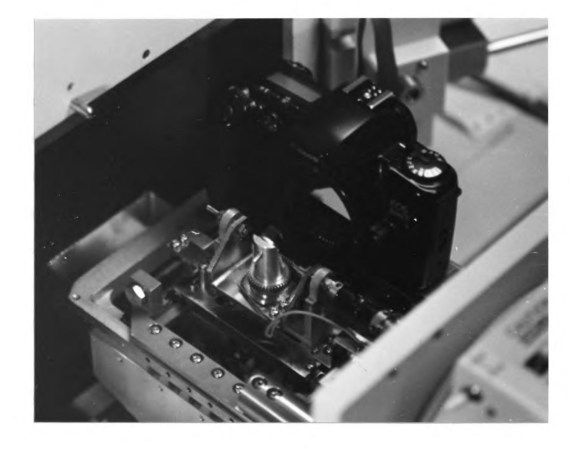


Figure 14

Specimen/camera configuration, shown in the retracted position, mounted on the SEM goniometer stage.

shutter release was wired through electrical feeds on the SEM chamber wall, enabling the activation of the shutter release externally without breaking vacuum. The button on the remote electronic cable shutter release was depressed for an appropriate amount of time, thus, activating the shutter and exposing the film to the backscattered electrons. The exact exposure times are noted in the individual experiments in Sections 2.5-2.5.3. The specimen-to-film distance was fixed at approximately 70 mm (to be discussed in more detail later) resulting in an EBSP angular field of approximately 20° vertical by 30° horizontal.

Kodak's Eastman Fine Grain Release Positive Film 5302 was found to be optimum for these studies. The 5302 film was purchased in 100 ft. rolls which were placed in an Alden 74 Bulk Film Daylight Loader that enabled the easy loading of 35mm cassettes, typically with approximately 36 frames. The film was securely fastened to the cassette spindle using either transparent tape or masking tape. Plastic 35mm cassettes with threaded, twist on end caps were used and proved to be very effective. After the film was loaded into the camera body in subdued light and the camera back was closed, the camera automatically unwound the film onto the opposite spindle and counted the number of frames that existed on the cassette. As pictures were taken (i.e. EBSPs were acquired), the film was motor wound back into the cassette one frame at a time. Therefore, when the last picture, or EBSP, was recorded, the film was completely rewound within its plastic cassette.

The 5302 film was developed for 4 minutes in undiluted Kodak D-19 developer under normal red safelight conditions. It was rinsed in Kodak indicator Stop Bath for 30 seconds prior to fixing in Kodak Rapid Fixer for 4 minutes followed by a 10

minute rinse in H<sub>2</sub>O and a final 5 second rinse in Kodak Photo-Flo. All photographic chemicals, including the final rinse Photo-Flo, were used at room temperature, usually near 75°F. Chemicals were mixed using distilled water to reduced any mineral deposits. All chemicals, except for the stop bath, were kept in 1 gallon Carboy containers and reused.

#### 2.3.2 LINK Merlin EBSP Camera System/Sample Set-up

A commercial LINK Merlin EBSP camera system was used for collecting EBSPs on-line. The system is comprised of a Merlin LTC 1162F40 low light television camera, LINK computer, camera control unit, and a digital link to a 486 PC. The PC contains a framegrabber board and Synoptics Limited, Semper<sup>TM</sup> 6.4 [57] image processing software.

The Semper hardware set-up consisted of 2 terminals, one of which was used to display Semper programming language and commands, and the other of which displayed the EBSP and any further processed EBSPs.

Semper commands used to capture, process, and save images to file were followed according to a Semper 6 Command Reference Guide [57].

Once video prints of the EBSPs were taken, 35mm pictures were taken of the video prints as they provided a longer lasting, more substantial print.

#### 2.4 Acquiring EBSPs

As will be discussed later, SEM parameters are very important in recording high quality EBSPs. In this study, an accelerating voltage of 25 kV, emission current of  $128 \pm 1 \mu A$ , a working distance of 28 mm when using the 35mm camera (and 10 mm when using the Merlin camera), and the #1 objective aperture of 300  $\mu$ m were

used while recording patterns. The condenser lens settings were chosen at the time of actual recording and varied between samples. However, the condenser lens settings that resulted in the brightest possible sample image were used.

In order to obtain an EBSP from a selected material, an area of the sample was selected from which EBSP information would be extracted. While in normal SEM secondary electron image mode, this chosen area was moved to the center of the viewing area. After switching from scanning mode to band mode, the cross hairs were moved to locate the exact position at which the electron beam would impinge the specimen. Just prior to switching to spot mode, the SEM was momentarily changed back to scanning mode for final focusing and condenser lens adjustment. In this scanning mode, the condenser lenses were changed to the lowest numerical setting possible that resulted in the brightest image possible. Spot mode was selected and the EBSP was recorded by either the LINK Merlin EBSP camera system or the 35mm camera system. When using the 35mm camera system, the exposure time varied between samples but was kept constant for all EBSPs recorded within each sample. When using the LINK Merlin EBSP camera system, the frame averaging times were kept constant for all EBSPs recorded. Again, the exact exposure times and frame averaging times are noted in the individual experiments' procedures.

In the experiments where EBSPs were recorded as a function of some distance, a duplicate of the SEM's digital micron marker was made on a piece of paper and taped to the screen at the location of the electron beam spot. This was done for each magnification used. This micron scale allowed for more accurate movement of the sample at the position of the electron beam spot.

#### **2.5 EBSP Experiments**

The preceding experiments have explained details and generalities of recording EBSPs. The following paragraphs explain the experiments conducted which aided in optimizing sample preparation procedures, EBSP recording and experimental techniques.

#### 2.5.1 Recording EBSPs using different films in the 35mm camera body

Using a GaAs sample, EBSPs were recorded on 4 different Kodak films using the 35mm camera body. EBSPs were exposed on Kodak's TMax<sup>TM</sup> 3200 film for 1.0 second, TMax<sup>TM</sup> 400 film for 10.0 seconds, Technical Pan<sup>TM</sup> film for 4.0 seconds, and Eastman Fine Grain Release Positive<sup>TM</sup> film for 10.0 seconds.

### 2.5.2 LINK Merlin EBSP Camera System vs. 35mm camera using GaAs and commercially pure Al specimens

The GaAs sample was prepared in accordance with 2.2.1 and placed in the SEM chamber initially aligned facing the plane of the Merlin camera.

Using the EBSP real-time acquisition process in Section 2.3.2, an EBSP was acquired and saved to a file. Another EBSP was obtained after further processing the EBSP image by frame averaging over 15 seconds.

Next, the specimen was rotated until its surface faced the plane of the 35mm camera film. Using the 35mm camera body and EBSP acquiring method discussed in Section 2.3.1, an EBSP was acquired with a 10 second exposure.

This experiment was then repeated using a sample of commercially pure Al.

## 2.5.3 EBSPs recorded after 5 minutes and after 25 minutes of electropolishing using a commercially pure Al specimen

The sample of commercially pure aluminum was prepared for electropolishing by the procedure outlined in Section 2.2.2. The sample was electropolished for 5 minutes. EBSPs were recorded from the sample using the 35mm camera body.

Next, the sample was further electropolished for an additional 20 minutes at the same electropotential settings which resulted in a total electropolishing time of 25 minutes, again, followed by the etching and rinsing procedure described above. EBSPs were again recorded from the sample. After film development and printing, visual comparisons of the EBSPs from the different electropolishing times were made.

2.5.4 EBSPs recorded as a function of distance away from a surface that has been damaged by mechanical grinding with a 180 grit sandbelt using a commercially pure Al specimen

After a cuboidal sample was cut using the Struers Accutom-5<sup>TM</sup> high speed cutoff machine, one surface of the sample was mechanically ground, using cooling water, on a 180 grit sandbelt. This provided the damaged surface as an origin (surface A depicted in Figure 15) away from which the EBSP study was performed.

An adjacent surface (surface B depicted in Figure 15) was then mechanically polished, electrolytically polished for 25 minutes, etched and rinsed in a manner described in Section 2.2.2. It was upon this surface, as a function of distance away from the damaged, mechanically ground surface, that EBSP analysis was performed. In a manner consistent with Section 2.5, using the taped micron marker as a guide, EBSPs were recorded at distances between 0.0 (the damaged surface origin) and 5.0

# ELECTROPOLISHED SURFACE UPON WHICH EBSPS WERE PERFORMED

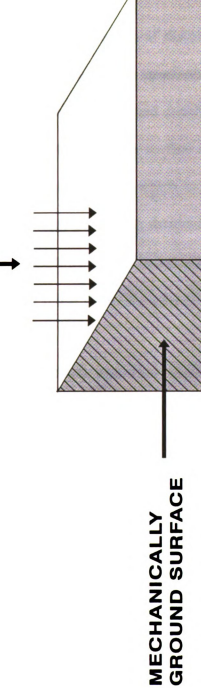


Figure 15

Commercially pure AI sample showing the mechanically ground surface and the electropolishing surface of interest upon which EBSPs were performed as a function of distance away from the damaged surface.

in 1.0 micron increments, between 8.0 and 12.0 in 2.0 micron increments, and between 15.0 and 30.0 in 5.0 micron increments.

After film development and printing, visual comparisons of the EBSPs were made.

## 2.5.5 EBSPs recorded as a function of distance away from an $(Al_2O_3)$ particulate in an $(Al_2O_3)$ ,/6061 aluminum alloy specimen

The specimen was heat treated and metallographically prepared as described in Section 2.2.2. Once in the SEM, the surface of the specimen was scanned so as to find a suitable (Al<sub>2</sub>O<sub>3</sub>) particulate on which to perform the EBSP experiment. It was necessary to find a solitary particulate surrounded by enough particulate-free matrix from which EBSP information could be extracted. The particulate-free matrix ensured that the strain fields from other particulates were not interfering with the quality of the EBSP.

Once the particulate was identified, EBSPs were recorded as function of distance away from the particulate/matrix interface, as depicted in Figure 16. In a manner consistent with Section 2.5, using the taped micron marker as a guide, EBSPs were recorded at 0.0 (the particulate/matrix interface origin), and at 1.0, 2.0, 5.0, and 8.0 microns away from the (Al<sub>2</sub>O<sub>3</sub>) particulate.

After film development and printing, visual comparisons of the EBSPs were made.

## ELECTROPOLISHED SURFACE UPON WHICH EBSPS WERE PERFORMED AWAY FROM AI<sub>2</sub>O<sub>3</sub> PARTICULATE

Figure 16

(Al<sub>2</sub>O<sub>3</sub>)/6061 aluminum matrix sample showing the (Al<sub>2</sub>O<sub>3</sub>) particulate away from which BBSPs were performed as a function of distance.

#### 3. EXPERIMENTAL RESULTS AND DISCUSSION

One goal of this study was to determine if the 35mm camera body system could be used to obtain EBSPs with some appropriate film. Additional goals lay in determining if the 35mm camera body system yields superior quality EBSPs as compared to the commercial LINK Merlin EBSP camera system and the effects of electropolishing on EBSP image quality.

As previously discussed, the delineation of the band edges is dependent upon crystalline perfection. Dislocations, and other defects such as stacking faults, are responsible for local bending of the lattice planes causing some electrons to be scattered away from this Bragg condition. This, in turn, results in an increased diffuseness of the band edges.

Therefore, one of the goals of this study is to qualify strain using the 35mm camera system. Strain, defined by local bending of the lattice planes, will be qualified by the increased diffuseness, or lack of delineation, of the edges of the electron backscattering pattern bands.

While examining prints of EBSP images, it should be noted that there is great difficulty in printing consecutive EBSP images with consistent levels of exposure. As discussed earlier, backscattered electrons originating from tilted specimens have a tendency for forward scattering. Therefore, the bottom portions of the Fine Grain Release Positive<sup>TM</sup> negative, as it sets in its position in the 35mm camera body, receive far more forward scattering backscattered electrons than do the top portions of the film. The exposure gradient results in weaker, lighter patterns at the top of the film and stronger, darker patterns at the bottom. Consequently, extensive dodging

techniques must be employed while printing to achieve any nominal level of consistency. Therefore, while visually studying the EBSP images, the deviations in exposure must be overlooked and concentration needs to be given to band edge delineation.

In order to facilitate visual comparisons between EBSPs, areas on many of the EBSP prints have been highlighted. Also note that there are faint horizontal scratches on the prints which may be due to the rubber squeegee originally used on the 35mm film. More recent studies do not include the use of the squeegee.

#### 3.1 EBSPs recorded on 4 different films

Prior to using the 35mm camera body in any experiments, it was necessary to determine the appropriate 35mm film for obtaining the highest quality EBSPs (i.e. contrast and resolution). Using a GaAs sample, EBSPs were recorded on 4 different films; Kodak's TMax<sup>TM</sup> 3200, TMax<sup>TM</sup> 400, Technical Pan<sup>TM</sup>, and Eastman Fine Grain Release Positive<sup>TM</sup> films are shown in Figure 17(a) - 17(d).

Kodak's TMax<sup>TM</sup> 3200 and TMax<sup>TM</sup> 400 films demonstrate excessive graininess as shown in Figure 17(a) and (b). Their graininess is obvious when compared to the EBSP images recorded on Kodak's Technical Pan<sup>TM</sup> and Fine Grain Release Positive<sup>TM</sup> films shown in Figures 17(c) and (d). Most of the finer band edges seen in Figure 17 (c) and (d) cannot be seen in Figures 17 (a) and (b).

The delineation of the band edges in the patterns recorded on Kodak's Technical Pan<sup>TM</sup> and Fine Grain Release Positive<sup>TM</sup> films, in Figures 17(c) and (d), is very sharp and is obviously superior to those of the other films.

The differences between Kodak's Technical Pan<sup>TM</sup> and Fine Grain Release

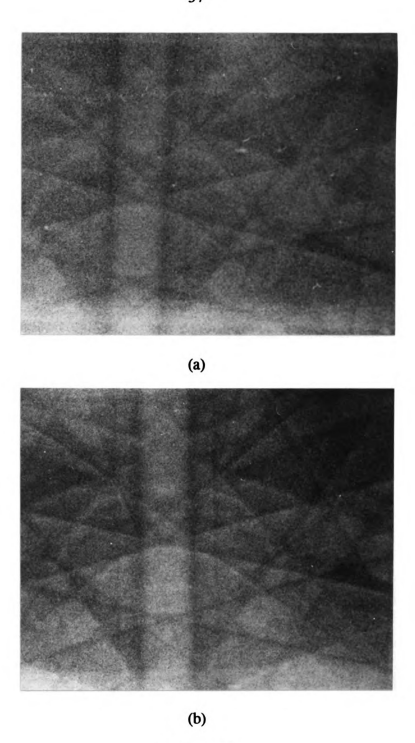


Figure 17

EBSP images of GaAs recorded with the 35mm camera body system, using Kodak's (a)  $TMax^{TM}$  3200, (b)  $TMax^{TM}$  400, (c) Technical  $Pan^{TM}$ , and (d) Fine Grain Release Positive<sup>TM</sup> film.

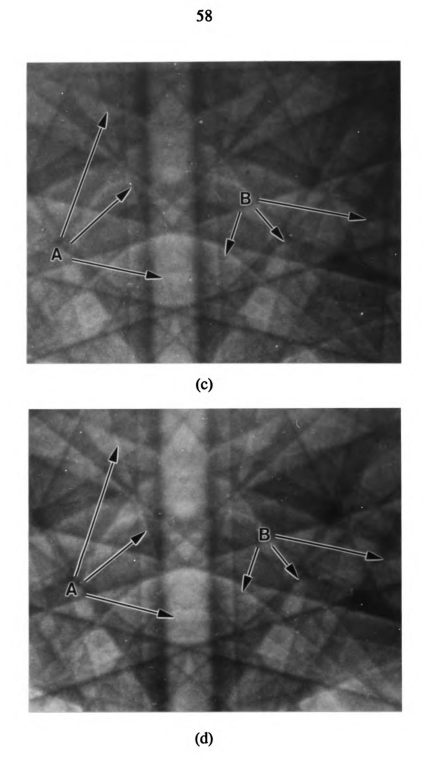


Figure 17 (cont'd).

Positive<sup>TM</sup> films are not so obvious and require closer scrutiny. Firstly, the Technical Pan<sup>TM</sup> film requires considerably shorter exposure times to achieve the same level of exposure. The actual negatives prove that an exposure of 10.0 seconds on Fine Grain Release Positive<sup>TM</sup> film yields the same level of exposure as 4.0 seconds of exposure on Technical Pan<sup>TM</sup> film. Therefore, if some contrast and resolution can be sacrificed for the advantage of shorter exposure times, Technical Pan<sup>TM</sup> film would be the film of choice. As discussed earlier, longer exposure times may result in surface contamination and pattern degradation problems due to hydrocarbon formation where the beam impinges the surface. Therefore, in order to determine which film demonstrates superior contrast and resolution, a more detailed study of band edges must be conducted.

In order to facilitate visual comparisons between the images shown in Figure 17(c) and (d), certain areas common to both images have been highlighted. In the EBSP recorded on Fine Grain Release Positive<sup>TM</sup> film, shown in Figure 17(d), there are two band edges highlighted by A and B. The faint band edge at A cannot be distinguished in Figure 17(c). The faint band edge at B, in Figure 17(d), barely can be resolved in Figure 17(c). This illustrates, along with the examination of other details in Figures 17(c) and (d), that the Fine Grain Release Positive<sup>TM</sup> film of Figure 17(d) has superior contrast than the Technical Pan<sup>TM</sup> film shown in Figure 17(c).

The brighter "bright" areas and darker "dark" areas in Figure 17(d) lend evidence to the superior contrast of the Fine Grain Release Positive<sup>TM</sup> film, but also help confuse the issue of resolution. After enlarging images from each type of film, it became obvious that the Fine Grain Release Positive<sup>TM</sup> film had a smaller grain size

than the Technical Pan<sup>TM</sup> film, and therefore, better resolution. The grain size of the Technical Pan<sup>TM</sup> film is dependent upon the type of film processing used. Other processing might produce a finer grain size than seen in this study.

Since contrast is of utmost importance in determining visually measurable differences in band edge diffuseness, Fine Grain Release Positive<sup>TM</sup> film is determined to be superior to Technical Pan<sup>TM</sup> film for this study.

## 3.2 LINK Merlin EBSP camera system vs. 35mm camera experiment using GaAs and commercially pure Al specimens

Once the appropriate film was determined, a comparison was made between the LINK Merlin EBSP camera system and the 35mm camera body system. Using the LINK Merlin EBSP camera system, an EBSP of GaAs was acquired, and saved to file. A video print was made of the "non-image processed" pattern. A 35mm picture of the video print is shown in Figure 18(a). To contrast the non-processed image, an EBSP was acquired after being "image processed" by frame averaging for 15 seconds using Semper 6.4 image processing software. A 35mm picture of the video print is shown in Figure 18(b). Next, an EBSP was recorded using the 35mm camera body system and is shown in Figure 18(c).

Figure 18(a) demonstrates the quality of the pattern achievable using the commercial LINK Merlin EBSP camera system with a GaAs specimen. Note that the images recorded using the Merlin EBSP camera reveal the edges of the phosphor scintillation screen as well as scratches in the phosphor coating. Typically, these images are very noisy, but may be improved by image processing using the Semper image processing software. Figure 18(b) demonstrates the quality of the pattern

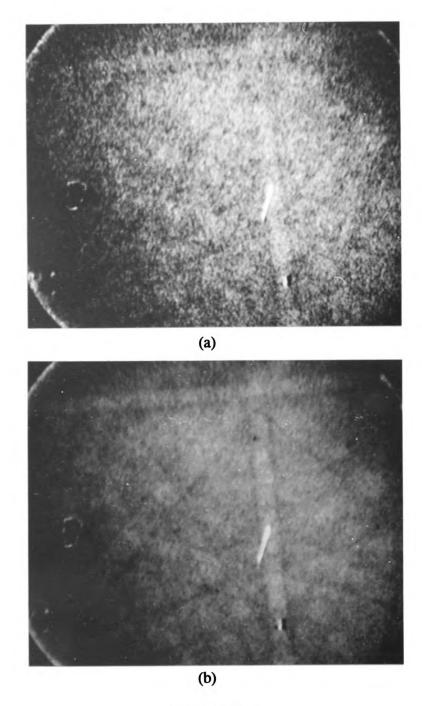


Figure 18

EBSP images of GaAs recorded using the (a) commercial LINK Merlin EBSP camera system with no image processing, (b) commercial LINK Merlin EBSP camera system coupled with Semper 6.4 image processing of 15 seconds of frame averaging, and (c) 35mm camera body system.

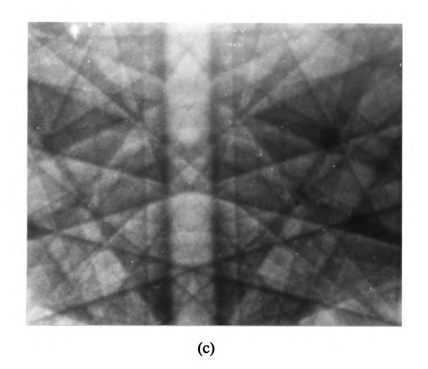


Figure 18 (cont'd).

achievable after 15.0 seconds of frame averaging. Much of the background noise has been eliminated and there is some improvement in overall contrast. Figure 18(b) represents the best image attainable with the commercial LINK Merlin EBSP camera system.

Figure 18(c) represents a typical image obtained using the 35mm camera body system. Its superior contrast and resolution, as compared to Figures 18(a) and (b) taken using the commercial system, is obvious. It should be noted that since the Merlin camera and 35mm camera body have different specimen normal-to-film angles and different specimen-to-film distances, Figure 18(c) represents the diffraction pattern somewhat differently than Figures 18(a) and (b).

Repeating the experiment using commercially pure aluminum, a 35mm picture of the "non-processed" EBSP video print is shown in Figure 19(a). A 35mm picture of the "image processed" EBSP video print is shown in Figure 19(b) and the EBSP recorded using the 35mm camera body system is shown in Figure 19(c). Figure 19(b) reveals improved contrast and overall image quality as compared to Figure 19(a). However, it falls far short of the quality shown in Figure 19(c) recorded using the 35mm camera body system.

Figures 18(c) and 19(c), taken using the 35mm camera body system, prove the overall superiority in contrast and resolution over that of the commercial LINK system. In some instances, where comparisons of the finer band edges may be needed to determine differences in strain, the images recorded using the commercial LINK system would be inadequate.

It should be noted that the commercial LINK system does have advantages. The

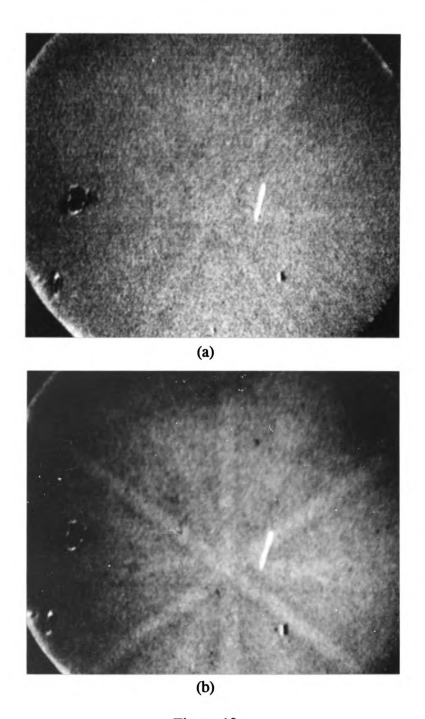


Figure 19

EBSP images of commercially pure AI recorded using the (a) commercial LINK Merlin EBSP camera system with no image processing, (b) commercial LINK Merlin EBSP camera system coupled with Semper 6.4 image processing of 15 seconds of frame averaging, and (c) 35mm camera body system.

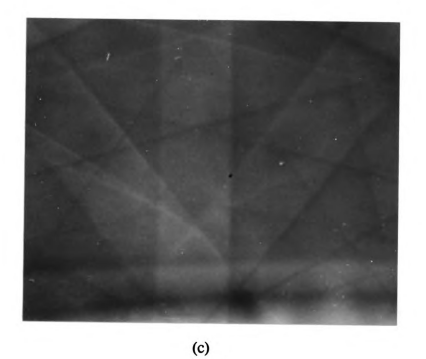


Figure 19 (cont'd).

LINK system provides real-time images of EBSPs that may be acceptable for certain applications using specimens of elements and alloys with higher atomic numbers.

Furthermore, the LINK computer allows for automatic indexing of EBSPs once at least 2 zones are manually identified.

## 3.3 EBSPs recorded after 5 minutes and after 25 minutes of electropolishing using a commercially pure Al specimen

Due to the importance of sample preparation in obtaining high quality EBSPs, an examination of the effects of electropolishing was conducted. After 5 minutes of electropolishing the commercially pure aluminum specimen, an EBSP was obtained using the 35mm camera body and is shown in Figure 20(a). All band edges shown are diffuse and lack definition. This diffuseness is characteristic of plastically deformed material containing local bending of the lattice planes. After an additional 20 minutes of electropolishing, for a total of 25 minutes, the band edges become extremely well defined as shown in Figure 20(b). Note that Figure 20(b) is an EBSP from a different grain although it was recorded from the same location on the sample. The differing patterns are a result of the first grain being electropolished away revealing a different grain underneath.

Even though the EBSPs were obtained from different grains, Figures 20(a) and (b) prove quite effectively the benefits of extended electropolishing in revealing material free of the deformation caused by mechanical polishing. The commercially pure Al sample, having undergone the mechanical polishing procedures described in Section 2.2.2, still contains considerable deformation as demonstrated by the lack of band edge delineation, shown in Figure 20(a). Therefore, brightness and reflectivity

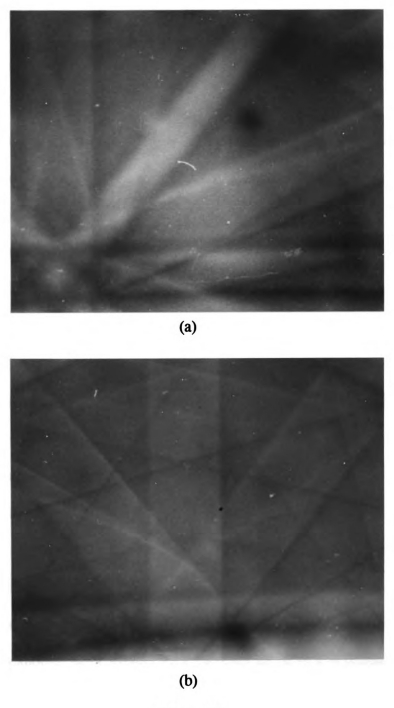


Figure 20

EBSP images of commercially pure AI recorded using the 35mm camera body system and Fine Grain Release Positive™ film after (a) 5 minutes of electropolishing (b) 25 minutes of electropolishing.

can be misleading indicators that the damage caused by mechanical polishing has been adequately removed. Figure 20(b) indicates, however, that 25 minutes of electropolishing reveals finely delineated band edges characteristic of material relatively free of deformation.

3.4 EBSPs recorded as a function of distance away from a surface that has been damaged by mechanical grinding with a 180 grit sandbelt using a commercially pure Al specimen

Having determined the feasibility of using the 35mm camera system in recording high quality EBSPs which are superior to those using the LINK Merlin EBSP camera systems, one of the goals of this study was to qualify strain using the 35mm camera system.

Strain, defined by local bending of the lattice planes, will be qualified by the increased diffuseness, or lack of delineation, of the edges of the electron backscattering pattern bands. When performing comparisons of EBSPs for the purpose of determining differences in strain, it is necessary to have bands, or portions of the EBSPs, common to all images. Certain crystallographic planes may be strained at the expense of, or to a greater degree than, other planes due to the alignment of their active slip systems. Comparing one EBSP band, formed from a particular set of (h k l) planes, to another band formed by a different set of (h k l) planes, would be committing a fundamental error. These different sets of (h k l) planes probably would not experience identical levels of deformation. Therefore, within the same EBSP image, one band might exhibit more diffuseness than another. So, comparing one band in one image to a different band in another image would not be scientifically

sound.

Along this same approach, individual grains may be deformed at the expense of, or to a greater degree than, other grains due to the alignment of their slip systems.

Therefore, it is important to conduct deformation studies within a single grain.

Consequently, in order to facilitate visual comparisons between the images shown in Figure 21, all recorded from the same grain, certain bands common to all images have been highlighted with capital letters.

As discussed in Section 2.5.4, EBSPs were recorded as a function of distance away from a damaged surface induced by mechanical grinding on a specimen of commercially pure aluminum. The EBSPs, recorded at distances between 0.0 (the damaged surface origin) and 5.0 in 1.0 micron increments, between 8.0 and 12.0 in 2.0 micron increments, and between 15.0 and 30.0 in 5.0 micron increments, are shown in Figures 21(a) - 21(l), respectively. Note that the EBSP recorded at 3.0 microns away from the damaged surface could not be produced into a usable print. It has been excluded from this study.

### Delineation of band edges

Note that the main visual feature, shown in Figures 21(a) - (l), is a horizontal EBSP band traversing the image.

Figure 21(a) was recorded at the mechanically damaged edge. In Figure 21(a), approximately 5 millimeters above and parallel to the main horizontal band, is a dark band edge, A, of another band. This edge is barely visible in the image.

Also, the general band edge quality in the entire image is poor, exhibiting diffuse band edges which is a characteristic of local bending of the lattice planes by

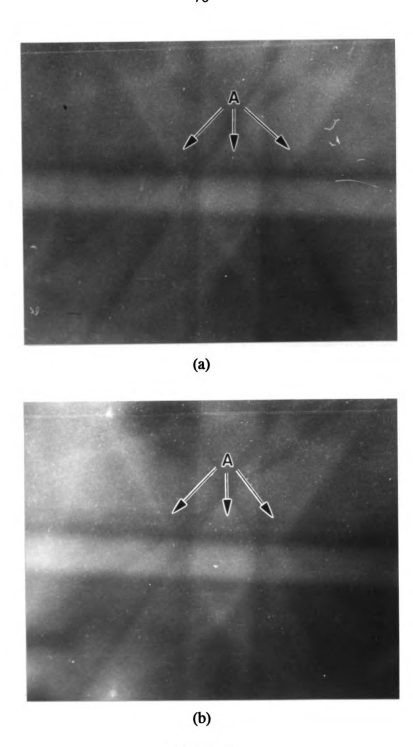


Figure 21

EBSP images of commercially pure Al recorded, using the 35mm camera body system and Fine Grain Release Positive  $^{TM}$  film, at (a) the damaged edge and (b) 1.0 micron away from the damaged edge.

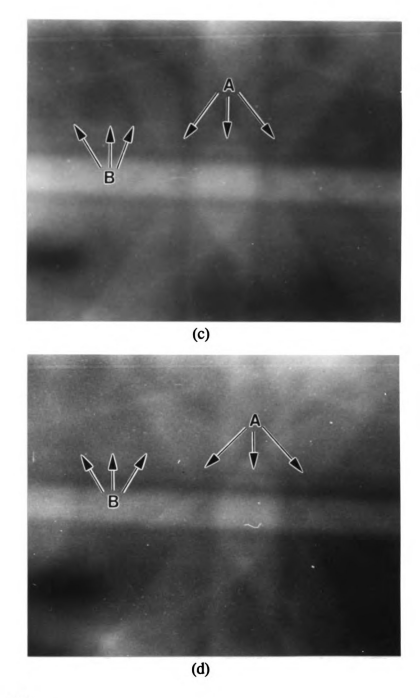


Figure 21 (cont'd).

EBSP images of commercially pure Al recorded, using the 35mm camera body system and Fine Grain Release Positive<sup>TM</sup> film, at distances of (c) 2.0 microns and (d) 4.0 microns away from the damaged edge.

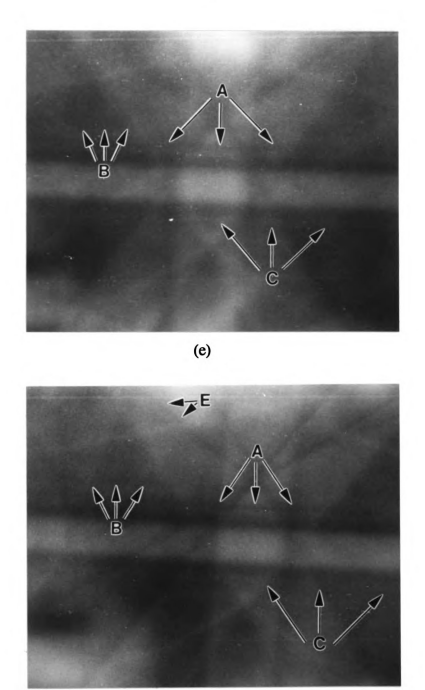


Figure 21 (cont'd).

EBSP images of commercially pure Al recorded, using the 35mm camera body system and Fine Grain Release Positive  $^{\text{TM}}$  film, at distances of (e) 5.0 microns and (f) 8.0 microns away from the damaged edge.

(f)

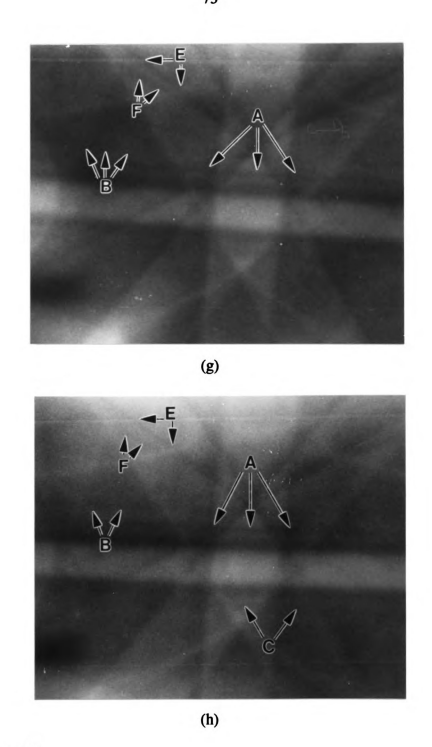


Figure 21 (cont'd).

EBSP images of commercially pure Al recorded, using the 35mm camera body system and Fine Grain Release  $Positive^{TM}$  film, at distances of (g) 10.0 microns and (h) 12.0 microns away from the damaged edge.

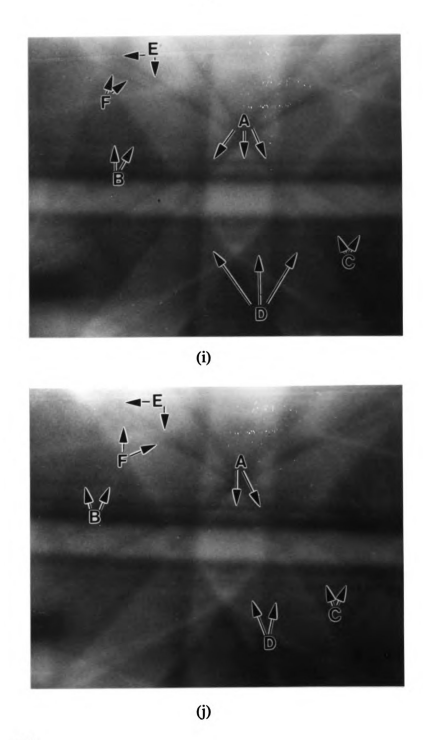


Figure 21 (cont'd).

EBSP images of commercially pure Al recorded, using the 35mm camera body system and Fine Grain Release Positive™ film, at distances of (i) 15.0 microns and (j) 20.0 microns away from the damaged edge.

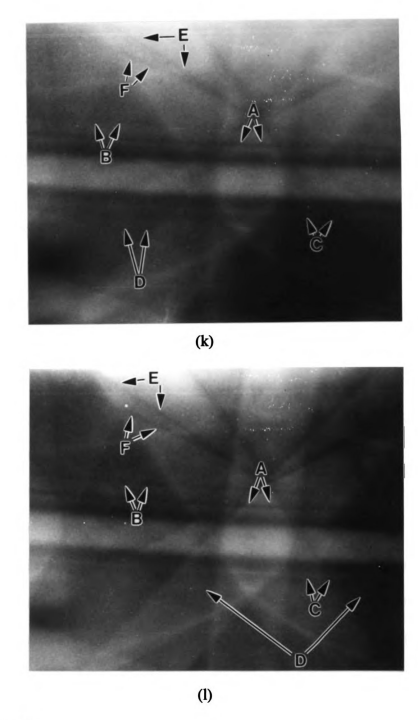


Figure 21 (cont'd).

EBSP images of commercially pure Al recorded, using the 35mm camera body system and Fine Grain Release Positive™ film, at distances of (k) 25.0 microns and (l) 30.0 microns away from the damaged edge.

strain away from Bragg conditions.

In Figure 21(b), recorded 1.0 micron away from the damaged edge, band edge A can be resolved to a slightly better degree. Figure 21(c), recorded 2.0 microns away from the damaged edge, demonstrates slight improvement in band edge A, as well as the appearance of a faint, diffuse dark band edge B. Band edge B lies approximately 5 millimeters above and parallel to band edge A. Recorded 4.0 microns away from the damaged edge, Figure 21(d), and 5.0 microns away, Figure 21(e), appear to have similar band edge qualities as Figure 21(c). However, Figure 21(e) contains the beginnings of a very faint bright band edge C. Bright band edge C accompanies dark band edge A, as discussed in Section 1.1, as the opposite edge of the same band.

Figure 21(f), recorded 8.0 microns away from the damaged edge, reveals very faint dark band edges E and F and a slightly better defined bright band edge C.

Figure 21(g), recorded 10.0 microns away from the damaged edge, reveals better defined dark band edges A, B, E, and F. The band edge qualities in Figure 21(h), recorded 12.0 microns away from the damaged edge, appear similar to those in Figure 21(g), except for an apparent washing out of band edge E. This washing out is probably due to incorrect shadowing. Figures 21(g) and (h) also lack the presence of band edge C. Once again, the fainter band edges, such as C, are easily washed out during printing procedures.

Figure 21(i), recorded 15.0 microns away from the damaged edge, demonstrates better contrasted band edges A, B, C, E, and F. Note the appearance of bright band edge D, which accompanies dark band edge B as the opposite edge of the same band.

Figures 21(j) and (k), recorded 20.0 and 25.0 microns, respectively, away from the damaged edge, demonstrate similar band edge quality as Figure 21(i).

Figure 21(1), recorded 30.0 microns away from the damaged edge, reveals better contrasted and more delineated bright and dark band edges. Bright band edges C and D are significantly sharper.

Visual observation of Figures 21(a) - (l) reveals steadily improving band edge contrast and delineation, and overall image quality, as images are recorded farther away from the damaged edge. This improvement in band edge quality is characteristic of a decrease in local lattice bending, i.e. less localized strain. The deformation/strain induced by mechanical grinding results in EBSP band edge diffuseness. The band edges become so diffuse, with increasing strain, they eventually disappear. Consequently, many of the band edges seen in the latter images are not present in the images taken closer to the damaged edge.

Though not within the scope of this present study, attempts have been made to quantify strain using EBSPs [41].

# 3.5 EBSPs recorded as a function of distance away from an $(Al_2O_3)$ particulate in an $(Al_2O_3)_p/6061$ aluminum alloy specimen

As discussed in Section 2.5.5, EBSPs were recorded as a function of distance away from an  $(Al_2O_3)$  particulate in a 6061 aluminum matrix. The EBSPs, recorded at 0.0 (the particulate/matrix interface origin) and at 1.0, 2.0, 5.0, and 8.0 microns away from the  $(Al_2O_3)$  particulate, are shown in Figures 22(a) - 22(e), respectively.

Figure 22(a), recorded from the matrix but at the  $(Al_2O_3)_p/6061$  matrix interface, reveals two different EBSPs, one containing the band A, and one containing band B.

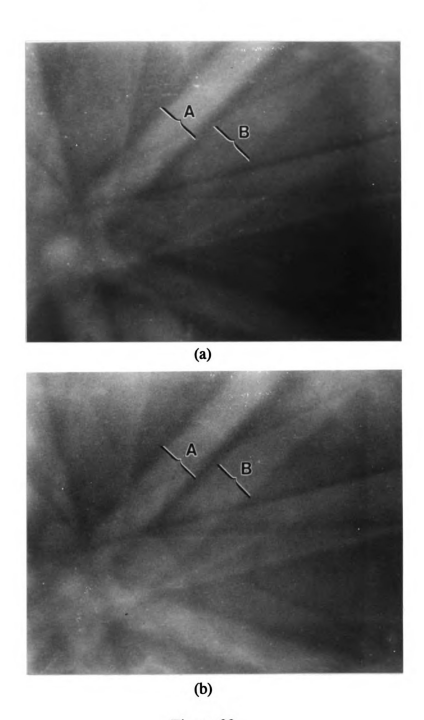


Figure 22

EBSP images of  $(Al_2O_3)_p/6061$  aluminum alloy, using the 35mm camera body system and Fine Grain Release Positive<sup>TM</sup> film, at (a) the  $(Al_2O_3)_p/6061$  matrix interface and (b) 1.0 micron away from the  $(Al_2O_3)_p/6061$  matrix interface.

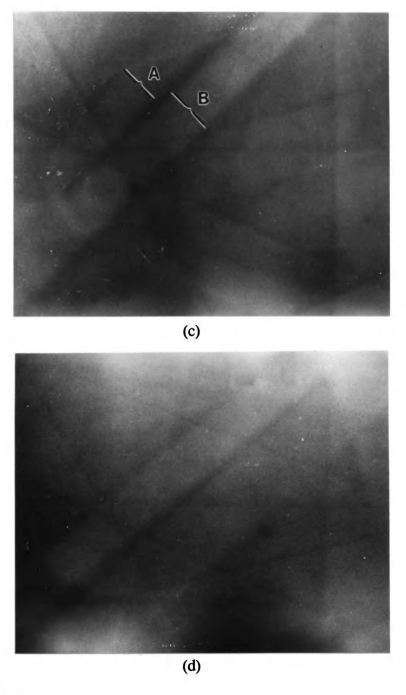


Figure 22 (cont'd).

EBSP images of  $(Al_2O_3)_{p'}/6061$  aluminum alloy recorded, using the 35mm camera body system and Fine Grain Release Positive<sup>TM</sup> film, at (c) 2.0 microns and (d) 5.0 microns away from the  $(Al_2O_3)_{p'}/6061$  matrix interface.

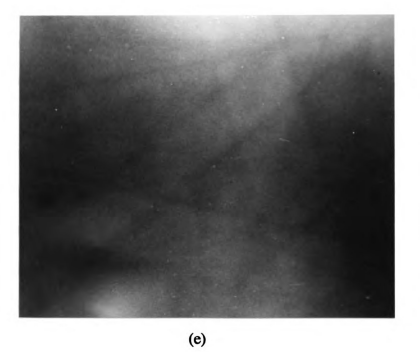


Figure 22 (cont'd).

EBSP images of  $(Al_2O_3)_p/6061$  aluminum alloy recorded, using the 35mm camera body system and Fine Grain Release Positive<sup>TM</sup> film, at (e) 8.0 microns away from the  $(Al_2O_3)_n/6061$  matrix interface.

Since these are two different EBSPs, they have originated from two different crystals. The interaction volume of the electron beam encompasses two different crystals, and therefore, yields diffraction information from both of the crystals. However, note that band A appears more prevalent than band B. Band A has better contrast and delineation as compared to band B. This can be understood, again, through the interaction volume of the electron beam. As more planes from a given set of (h k l) planes are involved in the Bragg diffraction of electrons, there is an increase in backscattered electrons contributing to the EBSP. Therefore, the image recorded appears brighter.

Figure 22(b), recorded 1.0 micron away from the (Al<sub>2</sub>O<sub>3</sub>)<sub>p</sub>/6061 matrix interface, discloses a band **B** with improved contrast and edge delineation. This is indicative of a larger electron beam interaction volume existing, within grain **B**, at 1.0 micron away from the interface than existed at the interface. Recorded 2.0 microns away from the interface, Figure 22(c) reveals band **B** becoming dominant, i.e. brighter with better contrast, over band **A**. Consequently, the electron beam interaction volume now encompasses more of the grain that is producing band **B** than the grain that is producing band **A**.

Figure 22(d), recorded 5.0 microns away from the (Al<sub>2</sub>O<sub>3</sub>)<sub>p</sub>/6061 matrix interface, contains EBSP diffraction information that, once again, differs from that contained in Figures 22(a) - (c). This is indicative of the diffraction information originating from different crystallographic volumes of material than either of the grains represented by the EBSPs in Figures 22(a) - (c). Note that Figure 22(d) also contains diffraction patterns from at least two different grains. Similar to Figure

22(d), Figure 22(e), recorded 8.0 microns away from the (Al<sub>2</sub>O<sub>3)<sub>p</sub>/6061 matrix interface, contains an electron backscattering pattern completely different from the previous four patterns.</sub>

Within a span of 8.0 microns away from the (Al<sub>2</sub>O<sub>3</sub>)<sub>p</sub>/6061 matrix interface, four completely different electron backscattering patterns are observed indicating that four different crystals are brought into interaction with the electron beam. This presents problems in the attempted EBSP analysis that cannot be overcome. As mentioned above, comparisons of EBSP quality for the purposes of determining differences in strain, cannot be made from one grain to another. Recall that grains may be deformed at the expense of, or to a greater degree than other grains due to the alignment of their active slip systems. Consequently, the delineation of a particular band in one grain cannot be compared to its delineation in another grain. The grain size of the 6061 aluminum alloy matrix is not large enough to use the EBSP technique for the purposes of determining strain as a function of distance away from an (Al<sub>2</sub>O<sub>3</sub>) particulate.

Alteration of the material's grain size may be possible using a cold work/anneal combination. However, the goal of this study was not to make the microstructure fit the EBSP analysis system, but to attempt the EBSP analysis on the material in the asreceived form.

### 4. CONCLUSIONS

Initial EBSP experiments comparing four different 35mm films proved that Kodak's Technical Pan<sup>TM</sup> and Fine Grain Release Positive<sup>TM</sup> films yielded superior quality. However, the Fine Grain Release Positive<sup>TM</sup> film showed better contrast and resolution at the expense of longer exposure times.

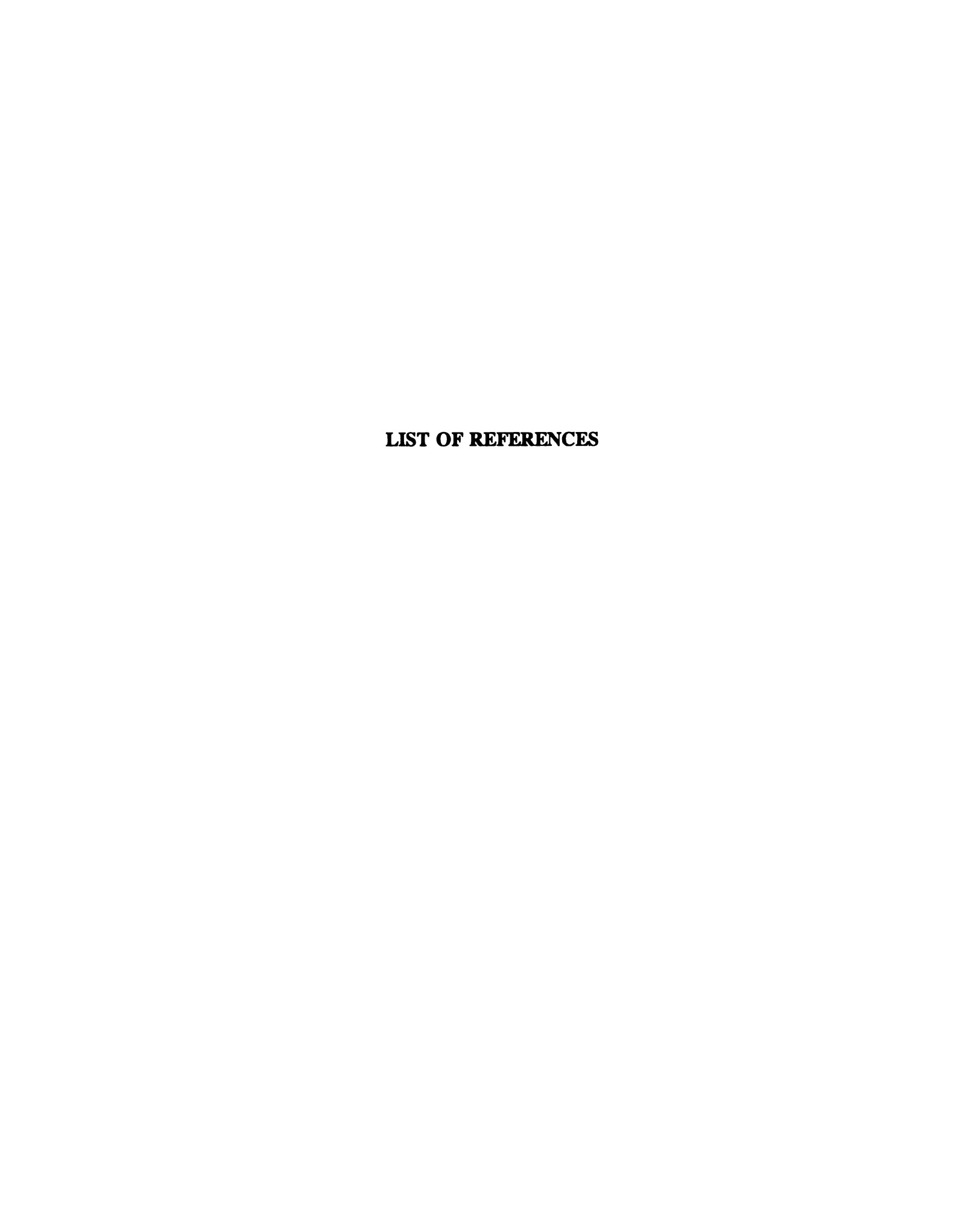
The 35mm camera system proved superior to the commercial LINK Merlin EBSP camera system in producing high quality images. Semper 6.4 image processing software, while yielding some improvements in image quality, could not raise image contrast and resolution to the high levels produced by the 35mm camera body system while obtaining EBSPs from a GaAs single crystal and a commercially pure aluminum specimen.

Electropolishing was seen to have important effects on EBSP quality. Extended electropolishing times, up to 25 minutes, result in extraordinary increases in EBSP quality. The improvement in EBSP contrast, resolution, and edge band delineation resulted from the removal of plastic deformation caused by mechanical grinding methods.

The 35mm camera body system proved successful in qualitatively analyzing strain in a commercially pure Al specimen. EBSP quality, measured by band edge delineation, improved gradually as a function of distance away from a surface that had been damaged by mechanical grinding.

In a final experiment, the EBSP technique was found inappropriate in determining strain as a function of distance away from an  $(Al_2O_3)$  particulate in an  $(Al_2O_3)_p/6061$  aluminum alloy, due to the small grain size of the matrix. EBSPs

could not be recorded from an individual grain for the purposes of band comparison.



#### LIST OF REFERENCES

- 1. Wischnitzer, S., <u>Introduction to Electron Microscopy</u>, Pergamon Press, New York, 1962.
- 2. Flegler, S., Heckman, J., Jr. and Klomparens, K., <u>Scanning and Transmission Electron Microscopy</u>, An Introduction, W.H. Freeman and Company, New York, 1993.
- 3. Goldstein, J., Newbury, D., Echlin, P., Joy, D., Romig, A., Jr., Lyman, C., Fiori, C. and Lifshin, E., Scanning Electron Microscopy, A Text for Biologist, Materials Scientists, and Geologists, Second Edition, Plenum Press, New York, 1992.
- 4. Dudarev, S., Rez, P. and Whelan, M., Theory of electron backscattering from crystals, Phys. Rev. B, Vol. 51, No. 6, 1 February 1995, pp. 3397-3412.
- 5. Reimer, L., Scanning Electron Microscopy- Physics of Image Formation and Microanalysis, Springer-Verlag, Berlin, 1985.
- 6. Joy, D., Monte Carlo Simulation in Turbo Pascal, University of Tennessee, 1993, computer program.
- 7. Gabriel, B., <u>SEM: A User's Manual for Materials Science</u>, American Society for Metals, Metals Park, Ohio, 1985.
- 8. Alam, M., Blackman, M. and Pashley, D., High-angle Kikuchi patterns, Proc. Royal Soc. London, Series A, Vol. 221, 1954, pp. 224-242.
- 9. Adams, B., Wright, S. and Kunze, K., Orientation Imaging: The emergence of a new microscopy, Metall. Trans. A, Vol. 24A, April 1993, pp. 819-831.
- 10. Venables, J. and Harland, C., Electron back-scattering patterns-A new technique for obtaining crystallographic information in the scanning electron microscope, Phil. Mag. 27, 1973, pp. 1193-1200.
- 11. Heimendahl, M., <u>Electron Microscopy of Materials</u>, <u>An Introduction</u>, Academic Press Limited, London, 1980.
- 12. Dingley, D. and Baba-Kishi, K., Electron backscatter diffraction in the scanning electron microscope, Microscopy and Analysis, Issue 17, May 1990.
- 13. Dingley, D. and Randle, V., Review-Microtexture determination by electron

- back-scatter diffraction, J. Mat. Sci., 27, 1992, pp. 4545-4566.
- 14. Dingley, D., Backscattering in the scanning electron microscope, Electron Microscopy and Analysis, Inst. Phys. Conf. Ser. No. 119, Sec. 13, 1991, pp. 551-558.
- 15. <u>LINK Analytical Technical Note</u>, Oxford Instruments Inc., Analytical Systems Division (formerly LINK), 130 A Baker Avenue Ext., Concord, MA 01742.
- 16. Bottcher, A., Hastenrath, M., Hjelen, J. and Lucke K., Nucleation-texture of early stages of primary recrystallization in electrical steel, Scripta Met. et Mater., Vol. 27, 1992, pp. 1115-1120.
- 17. Hjelen, J., Orsund, R. and Nes, E., On the origin of recrystallization textures in aluminum, Acta Metall. Mater., Vol 39, No. 7, 1991, pp. 1377-1404.
- 18. Troost, K., van der Sluis, P. and Gravesteijn, D., Microscale elastic-strain determination by backscatter Kikuchi diffraction in the scanning electron microscope, Appl. Phys. Lett. 62 (10), March 1993, pp. 1110-1112.
- 19. Wilkinson, A. and Dingley, D., The distribution of plastic deformation in a metal matrix composite caused by straining transverse to the fibre direction, Acta Metall. Mater., Vol. 40, No. 12, 1992, pp. 3357-3368.
- 20. Lee, W., Furley, J. and Ralph, B., Misorientation texture of post-recrystallized  $\alpha$ -brass, J. Mat. Sci., 27, 1992, pp. 3395-3399.
- 21. Wang, T., Morris, P. and Adams, B., Characterization of the morphological and lattice orientation microstructure of as-cast aluminum ingot, Metall. Trans. A, Vol. 21A, August 1990, pp. 2265-2275.
- 22. Michael, J. and Goehner R., Crystallographic phase identification in the scanning electron microscope:Backscattered electron Kikuchi patterns imaged with a CCD-based detector, Microsc. Soc. Amer. Bull., Vol. 23, No. 2, 1993, pp. 168-175.
- 23. Baudin, T. and Penelle, R., Determination of the total texture function from individual orientation measurements by electron backscattering pattern, Metall. Trans. A, Vol. 24A, October 1993, pp. 2299-2311.
- 24. Raabe, D. and Lucke, K., Annealing textures of bcc metals, Scripta Met. et Mater., Vol. 27, 1992, pp. 1533-1538.
- 25. Quested, P., Henderson, P. and McLean, M., Observations of deformation and fracture heterogeneities in a nickel-base superalloy using electron back

- scattering patterns, Acta Met., Vol. 36, No. 10, 1988, pp. 2743-2752.
- 26. Jensen, D., Hansen, N. and Humphreys, F., Texture development during recrystallization of aluminum containing large particles, Acta Met., Vol. 33, No. 12, 1985, pp. 2155-2162.
- 27. Randle, V., Ralph, B. and Dingley, D., The relationship between microtexture and grain boundary parameters, Acta Met., Vol. 36, No. 2, 1988, pp. 267-273.
- 28. Mason, T. and Adams, B., The application of orientation imaging microscopy, JOM, October, 1994, pp. 43-45.
- 29. Wright, S., Adams, B. and Kunze, K., Application of a new automatic lattice orientation measurement technique to polycrystalline aluminum, Mat. Sci. Eng., A160, 1993, pp. 229-240.
- 30. Doherty, R., Samajdar, I. and Kunze, K., Orientation Imaging Microscopy: Application to the study of cube recrystallization texture in aluminum, Scripta Met. et Mater., Vol. 27, 1992, pp. 1459-1464.
- 31. Dingley, D. and Baba-Kishi, K., Use of electron back scatter diffraction patterns for determination of crystal symmetry elements, SEM II, 1986, pp. 383-391.
- 32. Dingley, D., Alabaster, C. and Coville, R., Phase identification using backscatter Kikuchi diffraction in the scanning electron microscope, Inst. Phys. Conf. Ser. No. 98; Chpt. 10, 1989, pp. 451-454.
- 33. Wilkinson, A. and Dingley, D., Quantitative deformation studies using electron back scatter patterns, Acta Metall. Mater., Vol. 39, No. 12, 1991, pp. 3047-3055.
- 34. Wilkinson, A., Deformation studies of metal matrix composites using electron backscatter patterns, Mat. Sci. Eng., A135, 1991, pp. 189-193.
- 35. Wolf, E. and Hunsperger, R., Pseudo-Kikuchi pattern degradation of (111) gallium arsenide induced by 70-kev cadmium ion bombardment, Scanning Electron Microscopy, Proceedings of the Third Annual Scanning Electron Microscope Symposium, 1970, pp. 457-463.
- 36. Davidson, D., Uses of electron channelling in studying material deformation, Int. Met. Rev., Vol. 29, No. 2, 1984, pp. 75-95.
- 37. Dingley, D., Diffraction from sub-micron areas using electron backscattering

- in a scanning electron microscope, SEM II, 1984, pp. 569-575.
- 38. Stout, J., Texture and bimodal grain growth in B2 FeAl alloys, Master's Thesis, Michigan State University, Department of Materials Science and Mechanics, 1992.
- 39. Randle, V. and Powell, G., Application of electron backscatter diffraction to orientation measurements of individual carbides in a white cast iron, J. Mat. Sci. Lett., 12, 1993, pp. 779-781.
- 40. Gibson, A., Balcers, O. and Crimp, M.A., An economical method for obtaining high quality electron backscattered patterns using a 35mm camera body, submitted to J. of Microscopy, 1995.
- 41. Balcers, O., Master's Thesis, Michigan State University, 1995.
- 42. Lassen, N., Jensen, D. and Conradsen, K., Image processing procedures for analysis of electron backscattering patterns, Scanning Microscopy, Vol. 6, No. 1, 1992, pp. 115-121.
- 43. Wright, S. and Adams, B., Automatic analysis of electron backscatter diffraction patterns, Metall. Trans. A, Vol. 23A, March 1992, pp. 759-767.
- 44. Samuels, L., <u>Metallographic Polishing by Mechanical Methods</u>, 2nd Edition, American Elsevier Publishing Company, Inc., New York, 1971.
- 45. Harland, C, Akhter, P. and Venables, J., Accurate microcrystallography at high spatial resolution using electron back-scattering patterns in a field emission gun scanning electron microscope, J. Phys., E14, 1981, pp. 175-182.
- 46. Goodhew, P., <u>Specimen Preparation in Materials Science</u>, North-Holland Publishing Company, Amsterdam, 1972.
- 47. Metals Handbook, Ninth Edition, Vol. 9, <u>Metallography and Microstructures</u>, American Society for Metals, Metals Park, Ohio, 1985, pp. 49-50.
- 48. Tegart, W., <u>The Electrolytic and Chemical Polishing of Metals</u>, Pergamon Press, London, 1959.
- 49. Metals Handbook, American Society for Metals, Metals Park, Ohio, 1948, pg. 798.
- 50. Grummon, D., private communication with author, January, 1995.
- 51. Wilkinson, A., private E-mail with author, January, 1995.

- 52. Davies, J., Friesen, J. and McIntyre, J., A radiochemical technique for studying range-energy relationships for heavy ions of keV energies in aluminum, Can. J. Chem., Vol. 38, 1960, pp. 1526-1534.
- 53. Kornelsen, E., Brown, F., Davies, J., Domeij, B. and Piercy, G., Penetration of heavy ions of keV energies into monocrystalline tungsten, Phys. Rev., Vol. 136, No. 3A, November, 1964, pp. 849-858.
- 54. Davies, J., Ball, G., Brown, F. and Domeij, B., Range of energetic Xe<sup>125</sup> ions in monocrystalline silicon, Can. J. Phys., Vol. 42, June, 1964, pp. 1070-1080.
- 55. Davies, J., Brown, F. and McCargo, M., Range of Xe<sup>133</sup> and Ar<sup>41</sup> ions of kiloelectron volt energies in aluminum, Can. J. of Phys., Vol. 41, 1963, pp. 829-843.
- 56. Lee, J., Subramanian, K. & Kim, Y. (1994); The interface in Al<sub>2</sub>O<sub>3</sub> particulate reinforced aluminum alloy composite and its role on the tensile properties, J. Mat. Sci., 29, pp. 1983-1990.
- 57. Synoptics Limited, Semper 6 Command Reference Guide, 271 Cambridge Science Park, Milton Road, Cambridge, CB4 4WE, UK.

